Interaction between hydrothermal fluids and fault systems in the in the Southern Andes revealed by magnetotelluric and seismic data

R. K. Pearce[1], Almudena Sánchez de la Muela[2], Max Moorkamp[3], J. O. S. Hammond[2], Thomas M. Mitchell[1], José Cembrano[4], Jaime Araya Vargas[5], Philip G. Meredith[1], Pablo Iturrieta[5], Nicólas Pérez-Estay[6], Neill Marshall[7], Gonzalo Yañez[5], Ashley Griffith[8], Carlos Marquardt[5], Jonathan Smith[9], Ashley Stanton-Yonge[1], and Rocio Núñez[5]

[1]University College London
[2]Birkbeck
[3]Ludwig Maximilians Universitaet
[4]Pontificia Universidad Católica de Chile
[5]Pontificia Universidad Católica
[6]Andean Geothermal Center of Excellence (CEGA)
[7]Oxford University
[8]Ohio State University
[9]California Institute of Technology

November 21, 2022

Abstract

In an active volcanic arc, magmatically sourced fluids are channeled through the brittle crust by structural features. This interaction is observed in the Andean volcanic mountain belt, where volcanoes, geothermal springs and the locations of major mineral deposits coincide with NNE-striking, convergent margin-parallel faults and margin-oblique, NW/SE-striking Andean Transverse Faults (ATF). The Tinguiririca and Planchón-Peteroa volcanoes in the Andean Southern Volcanic Zone (SVZ) demonstrate this relationship, as both volcanic complexes and their spatially associated thermal springs show strike alignment to the outcropping NNE oriented El Fierro Thrust Fault System. This study aims to constrain the 3D architecture of this fault system and its interaction with volcanically sourced hydrothermal fluids from a combined magnetotelluric (MT) and seismicity survey. The 3D conductivity model and seismic hypocenter locations show correlations between strong conductivity contrasts and seismic clusters in the top 10km of the crust. This includes a distinct WNW-striking seismogenic feature which has characteristics of the ATF domains. As the surveyed region is characterized by high heat flow regimes, volcanic activity and hydrothermal systems related to the volcanic arc, the conductivity contrast suggests that magmatically derived fluids meet an impenetrable barrier, most likely the sealed core of the fault. The resulting increase in hydrostatic fluid pressure facilitates seismic activity on this WNW oriented structure. These results provides the first observation of the mechanism behind the reactivation and seismogenesis of ATF. The study also uncovers the role of the ATF the compartmentalization of magmatic-derived fluids that accumulate to form hydrothermal reservoirs in the SVZ.

Interaction between hydrothermal fluids and fault systems in the in the Southern Andes revealed by magnetotelluric and seismic data

R. K. Pearce [1], A. Sánchez de la Muela [2,1], M. Moorkamp [3], J. O. S. Hammond [2], T. M. Mitchell [1], J. Cembrano [4], J. Araya Vargas [4,5], P. G. Meredith [1], P. Iturrieta [6], N. Pérez Estay [5], N. R. Marshall [7], J. Smith [8], G. Yañez [4], W. Ashley Griffith [9], C. Marquardt-Román [4], A. Stanton-Yonge [1,4], R. Núñez [4]

[1]Earth Science, University College London, London, United Kingdom
[2]Department of Earth and Planetary Sciences, Birkbeck, University of London, London, United Kingdom
[3]Earth and Environmental Sciences, Ludwig-Maximilians-Universität München, Munich, Germany
[4]Dept. Ingeniería Estructural y Geotécnica, Pontificia Universidad Católica de Chile, Santiago, Chile
[5]Centro de Excelencia en Geotermia de los Andes (CEGA), Universidad de Chile, Santiago, Chile
[6]Helmholtz Centre Potsdam, GFZ German Research Centre for Geosciences, Potsdam, Germany
[7]Department of Earth Sciences, University of Oxford, Oxford, United Kingdom
[8]Division of Geological and Planetary Sciences, California Institute of Technology
[9]School of Earth Sciences, Ohio State University, Columbus, OH, USA

Key Points:

- Margin parallel and oblique structures exert control on Andean volcanic and hydrothermal processes
- A dense magnetotelluric and seismic survey maps these processes in the shallow (<20km) crust
- Results show volcanic fluids are compartmentalized by local fault systems, and induce seismogenesis

Corresponding author: R. K. Pearce, `r.pearce.11@ucl.ac.uk`

Abstract

[In an active volcanic arc, magmatically sourced fluids are channeled through the brittle crust by structural features. This interaction is observed in the Andean volcanic mountain belt, where volcanoes, geothermal springs and the locations of major mineral deposits coincide with NNE-striking, convergent margin-parallel faults and margin-oblique, NW/SE-striking Andean Transverse Faults (ATF). The Tinguiririca and Planchn-Peteroa volcanoes in the Andean Southern Volcanic Zone (SVZ) demonstrate this relationship, as both volcanic complexes and their spatially associated thermal springs show strike alignment to the outcropping NNE oriented El Fierro Thrust Fault System. This study aims to constrain the 3D architecture of this fault system and its interaction with volcanically sourced hydrothermal fluids from a combined magnetotelluric (MT) and seismicity survey. The 3D conductivity model and seismic hypocenter locations show correlations between strong conductivity contrasts and seismic clusters in the top 10km of the crust. This includes a distinct WNW-striking seismogenic feature which has characteristics of the ATF domains. As the surveyed region is characterized by high heat flow regimes, volcanic activity and hydrothermal systems related to the volcanic arc, the conductivity contrast suggests that magmatically derived fluids meet an impenetrable barrier, most likely the sealed core of the fault. The resulting increase in hydrostatic fluid pressure facilitates seismic activity on this WNW oriented structure. These results provides the first observation of the mechanism behind the reactivation and seismogenesis of ATF. The study also uncovers the role of the ATF the compartmentalization of magmatic-derived fluids that accumulate to form hydrothermal reservoirs in the SVZ.]

1 Introduction

The ascent of magmatically sourced fluids through the brittle crust is facilitated by inherited planes of weakness, such as lithospheric scale fault systems (Nakamura, 1977; Shaw, 1980; Cembrano & Lara, 2009). Within these fault systems, highly permeable networks of inter-connected fault damage zones act as fluid conduits, whereas the low-permeability fault cores inhibit cross-fault fluid flow. This occurs as variations in pressure, temperature and composition of fluids in the fracture network can lead to fracture sealing and cementation due to mineral precipitation during fluid transport, which decreases the permeability of the fault core (e.g. Cox, 2005; Micklethwaite et al., 2010). This causes the maximum flow direction to orient parallel to the fault plane (Caine et al., 1996; D. Faulkner et al., 2011). Simultaneously, the migration and accumulation of fluids within these fault systems exert an essential role in the nucleation of earthquakes, as increased pore fluid pressures reduce the effective normal stress projected on a fault plane, consequently increasing its probability of failure (Sibson, 1985; Cox, 2010, 2016; Roquer et al., 2017). These interdependent processes result in episodic and anisotropic migration of fluids within a fault zone, along with the heterogeneous distribution of hydro-mechanical properties therein (Sibson, 1996, 2004; J. Rowland & Sibson, 2004; Cox, 2010).

In an active volcanic arc, this complex interaction between hydrothermal fluids and structural systems can significantly influence tectono-magmatic processes, such as the distribution of volcanoes (Nakamura, 1977; Tibaldi, 2005; Cembrano & Lara, 2009; Sielfeld et al., 2016), the emplacement of ore deposits and plutons (Hedenquist & Lowenstern, 1994; Piquer et al., 2016), the localized structural and geochemical development of geothermal springs and fumaroles (Sibson, 1996; Sánchez et al., 2013; Tardani et al., 2016) and the location, magnitudes, frequency and timing of crustal seismicity (Cox, 2016). Geophysical studies can image these active structural and hydromagmatic systems, in order to map their architecture as a function of depth. In particular, magnetotelluric (MT) surveys map electrical conductivity domains that are commonly related to the presence/absence of fluids with different degrees of salinity or partial melt at a crustal scale (Simpson & Bahr, 2005; Pommier, 2014). When combined with local seismic hypocenter locations, the spatial coherency of anomalous conductors and seismogenic features can reveal interacting hydrothermal fluids

77 and seismically active fault systems in a volcanic regime (Wannamaker et al., 2009; Becken
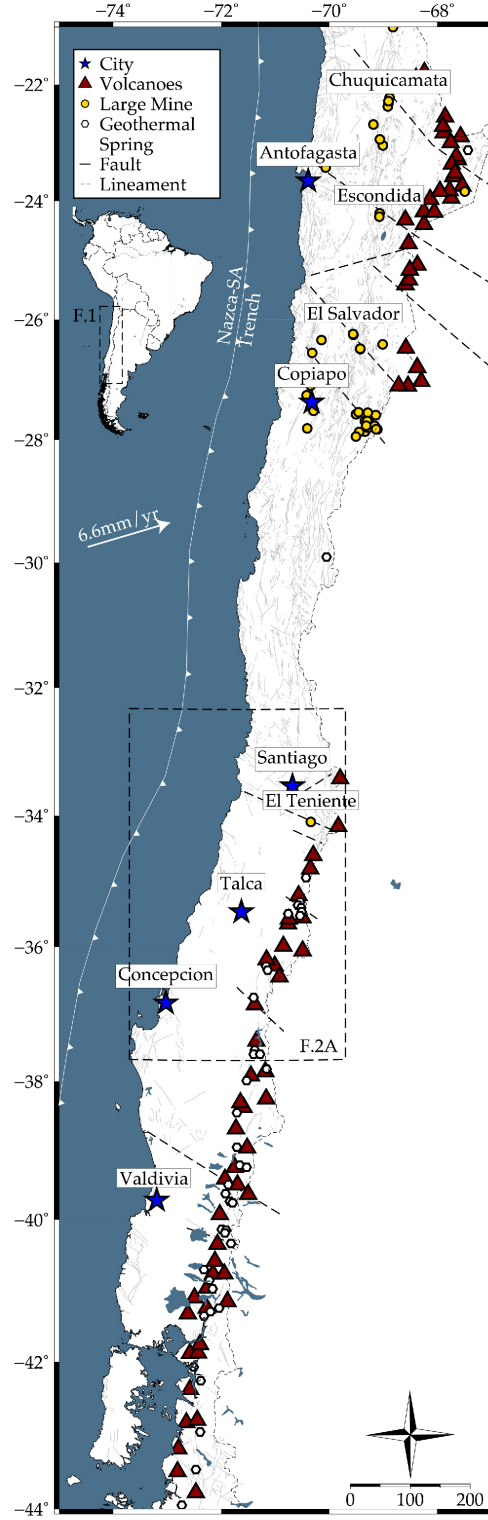78 et al., 2011; Bertrand et al., 2012).

79 The overall aim of this study is to image the architecture of a structural system
80 within a volcanic arc, and analyze the relation between its active deformation and fluid
81 transport/storage processes throughout the upper crust. This was achieved by conducting
82 spatially-overlapping MT and seismic surveys in the Andean Southern Volcanic Zone (SVZ).
83 The selected field study area encompasses the Tinguiririca and Planchón-Peteroa Volcanic
84 complexes (70.4 - 70.9°W and 34.65 - 35.2°S), where interdependent tectonic-hydrothermal
85 processes are evident from the following features: the region around Tinguiririca has been
86 considered for geothermal energy exploitation due to the prominent geothermal reservoir
87 found at the western flank of the volcanic complex (Clavero et al., 2011; Pritchard et al.,
88 2013; Aravena et al., 2016; Benavente et al., 2016), Planchón-Peteroa has been episodi-
89 cally on yellow alert due to degassing and ash expulsion events since 2011 (Aguilera et al.,
90 2016; Global-Volcanism-Program, 2019), and the volcanoes and proximal geothermal springs
91 demonstrate NNE-strike alignment along the major El Fierro Fault System (EFFS) system
92 that outcrops within the field area (Pavez et al., 2016; Giambiagi et al., 2019). Further-
93 more, this region of the SVZ is of particular interest due to the presence of both convergent
94 margin-parallel fold-thrust belt systems such as the EFFS, and margin-oblique WNW - ENE
95 striking features, referred to as Andean Transverse Faults (ATF) (Katz, 1971; Cembrano &
96 Lara, 2009). Although significant geological and geochemical evidence indicates that these
97 margin-oblique structures exert control on volcanism (Lara et al., 2004; Cembrano & Lara,
98 2009; Sielfeld et al., 2016; Piquer et al., 2019), hydrothermal system dynamics (Lara et al.,
99 2004; Sanchez-Alfaro et al., 2015) and ore-porphyry deposition (Sillitoe, 1997; Chernicoff
100 et al., 2002), the subsurface interaction of these processes are poorly understood. These
101 structural systems are here discussed in further detail.

1.1 Margin parallel and oblique fault systems in the Southern Andes

103 The Andes comprise of a NNE-SSW trending volcanic mountain chain along the western
104 margin of South America between latitudes 18-46°S, which have formed from the eastward
105 dextral-oblique convergence and subduction of the oceanic Nazca Plate beneath the South
106 American Plate since the Jurassic (ca 180Ma) (Pardo et al., 1967; Mpodozis et al., 1989;
107 Charrier et al., 2007; Ramos, 2010). Since 20Ma, orogenic uplift was coupled with episodes
108 of extension, intense volcanism and the formation of an eastward migrating volcanic arc at a
109 relative plate convergence velocity of 6.6cm/year along a trend of N78°E (Angermann et al.,
110 1999). The Andean western margin is characterized by: (a) over 200 tertiary stratovolcanoes
111 throughout its volcanic arc (60 of which have been active during the Holocene) (Stern et
112 al., 2007), (b) Mega-thrust earthquakes that reach magnitudes >Mw8, such as the Mw9.6
113 Valdivia and Mw 8.9 Concepcion earthquakes in 1960 and 2010 respectively (Bonali et al.,
114 2013), (c) giant Cu±Au±Ag porphyry ore deposits (Sillitoe, 1997; Chernicoff et al., 2002),
115 (d) and 431 ±321 MWe of potential high enthalpy geothermal resources (Sanchez-Alfaro
116 et al., 2015; Aravena et al., 2016). Figure 1 shows the major NNE trending and margin-
117 parallel volcanic arc and the distribution of ore deposits, geothermal springs and oblique
118 lineaments along the Andes. Throughout this region volcanoes, geothermal springs and the
119 locations of major mineral deposits are spatially coherent with the first-order NNE oriented
120 structural systems in the High Andes (Ramos, 2010), excepting the region between 28 - 33°S
121 referred to as the Pampean Flat Slab Segment, where shallow subduction angles prevented
122 the formation of a mantle wedge, resulting in a break in the volcanic arc (Mpodozis et al.,
123 1989).

124 Second order NW-trending transverse structural domains that cross-cut the volcanic
125 orogeny have been observed throughout the Andes, and they are considered to be pre-
126 Andean, inherited basement faults (Katz, 1971; Yáñez et al., 1998; Melnick & Echtler,
127 2006). These seismically active Andean Transverse Faults (ATF) (Aron et al., 2015; Stanton-
128 Yonge et al., 2016; Sielfeld et al., 2019) are enigmatic due to their severe misorientation to

Figure 1. Map of the Andean volcanic chain between latitudes 21.5° and 44°S. See key in top left corner for description of symbols. This includes active volcanoes from the Smithsonian Institute Holocene Volcanic database, geothermal areas from (Aravena et al., 2016), faults and major mines from Sernageomin (2003), northern lineaments (21.5-28°S) sourced from Richards et al. (2001), southern lineaments from Cembrano and Lara (2009)), and plate vector from Angermann et al. (1999). The frame overlying the map between latitudes 32-38°S indicates the location of Figure 2a.

the current plate convergence vector, which promotes a compressive stress regime and thus makes them unfavourable for seismic activity (Cembrano & Lara, 2009; Stanton-Yonge et al., 2016). As their surface expression is limited except a few scarce outcrops (Lara et al., 2004; Pérez-Flores et al., 2016), ATF have been inferred based on kilometer scale topographic lineaments (Cembrano & Lara, 2009; Piquer et al., 2016; Giambiagi et al., 2019) and alignment of seismicity and volcanic strikes (Lara et al., 2004; Aron et al., 2015; Sielfeld et al., 2016).

The intersection of major NNE oriented fault systems and the potentially blind, discrete WNW-striking ATF domains occur across all latitudes of the Andes, showing an along-strike spatial control of major mineral deposits (Katz, 1971; Sillitoe, 1997). Sillitoe (1997) & Piquer et al. (2019) suggested that hydrothermal minerals related to porphyry copper deposits of central Chile are precipitated at such intersections. Furthermore, ATF are considered to influence magmatic processes, as volcanic and intrusive body emplacement show alignment with the strike of ATF domains (Viramonte et al., 1984; Cembrano & Lara, 2009; Acocella et al., 2011). More recent investigations have determined that these structures store over-pressurized fluids derived from deep magmatic roots, thus impacting the architecture and distribution of active volcanic and hydrothermal systems (Sánchez et al., 2013; Wrage et al., 2017; Sielfeld et al., 2019). Furthermore, the interaction between NNE fault systems and ATF at the SVZ controls the conditions required to develop and sustain a shallow hydrothermal system, where fluids within conduits associated with ATF are stored and over-pressurized (Pérez-Flores et al., 2017; Roquer et al., 2017).
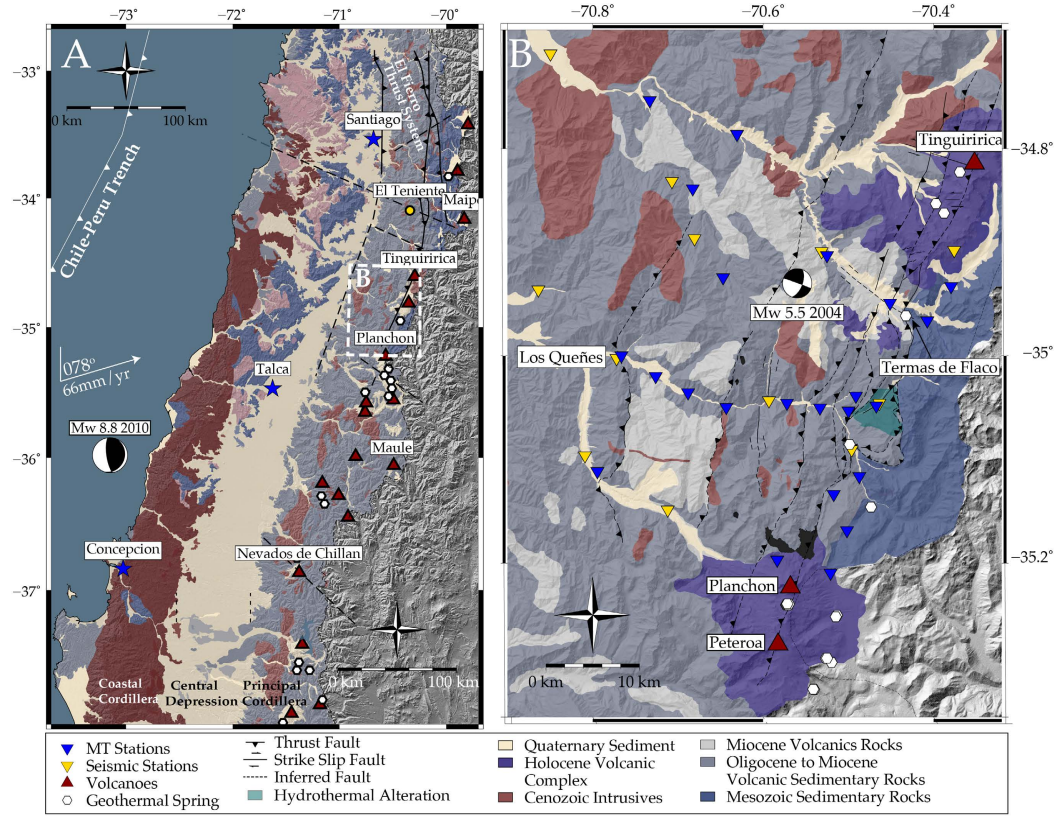
The setting of this study in the Andean SVZ thus includes the convergent-margin parallel fault systems, margin oblique ATF system, and fault-strike aligned volcanic complexes. The surface expressions, geophysical and geochemical signatures of these domains attest to their complex, interdependent, orogenic processes, yet their in situ interaction at depth remains unresolved. This study will provide a high-resolution 3D model of an area that is characterized by these structural and volcanic systems, in order to improve our understanding of their nature within upper crustal depths.

2 Regional context and geology

The Chilean Andes are segmented from north to south into the Northern, Central, Southern and Austral Volcanic Zones, due to the latitudinal variation of altitude, crustal thickness, convergence rate, plate coupling, volcanism and climate (Ramos, 2010). The selected field area for this study is in the Southern Volcanic Zone (SVZ) in the Principal Cordillera (Figure 2a). In this region, the main morpho-tectonic features of the Chilean Andes are the western coastal and eastern Principal Cordillera, which are divided by the Central Depression (Figure 2a) (Charrier et al., 2014; Ramos et al., 2014). The NNE striking EFFS is the major structural feature in the region, which thrusts the Miocene volcanic sequences eastward over an exposed sequence of Mesozoic sedimentary units (Farías et al., 2010). The surveyed study area is located at the western limit of the Chilean Principal Cordillera at this Meso-Cenozoic boundary (Figure 2b) (Núñez, 2018). This boundary is characterized by a heat flow regime of $200mW/m^2$, which is anomalously high compared to the heat flow regime of $60mW/m^2$ in the surrounding western and north-western Andes. This occurs as the eastward migrating volcanic arc is partially situated beneath the Principle Cordillera. Thus volcano-magmatic processes, such as the development of major stratovolcanoes and geothermal fluid outflow springs, are concentrated in the High Andes (Figure 1) (Benavente et al., 2016). The Tinguiririca geothermal outflow spring, as well as the Planchón-Peteroa volcanic complex are within the limits of the geophysical survey grid.

2.1 Tinguiririca and Planchón-Peteroa Stratovolcanic Complexes

The Tinguiririca volcanic complex is a Holocene cluster of 10 scoria cones that overly a lower to middle Pleistocene plateau of andesitic lavas (Stern et al., 2007). Current evidence

Figure 2. A) Regional scale geology of the southern volcanic zone of the Andean volcanic mountain belt. See legend for a description of all symbols. The geological units and the El Teniente mine location are after Sernageomin (2003), focal mechanisms of the Maule and Teno earthquakes are after Ekstrm, 2012. Frame labelled B in A indicate the location of Figure 2B. B) Local geological map of the field study area is from Núñez (2018) and distribution of magnetotelluric and seismic stations within the geophysical survey grid. Digital Elevation Model (DEM) from PALSAR (2011).
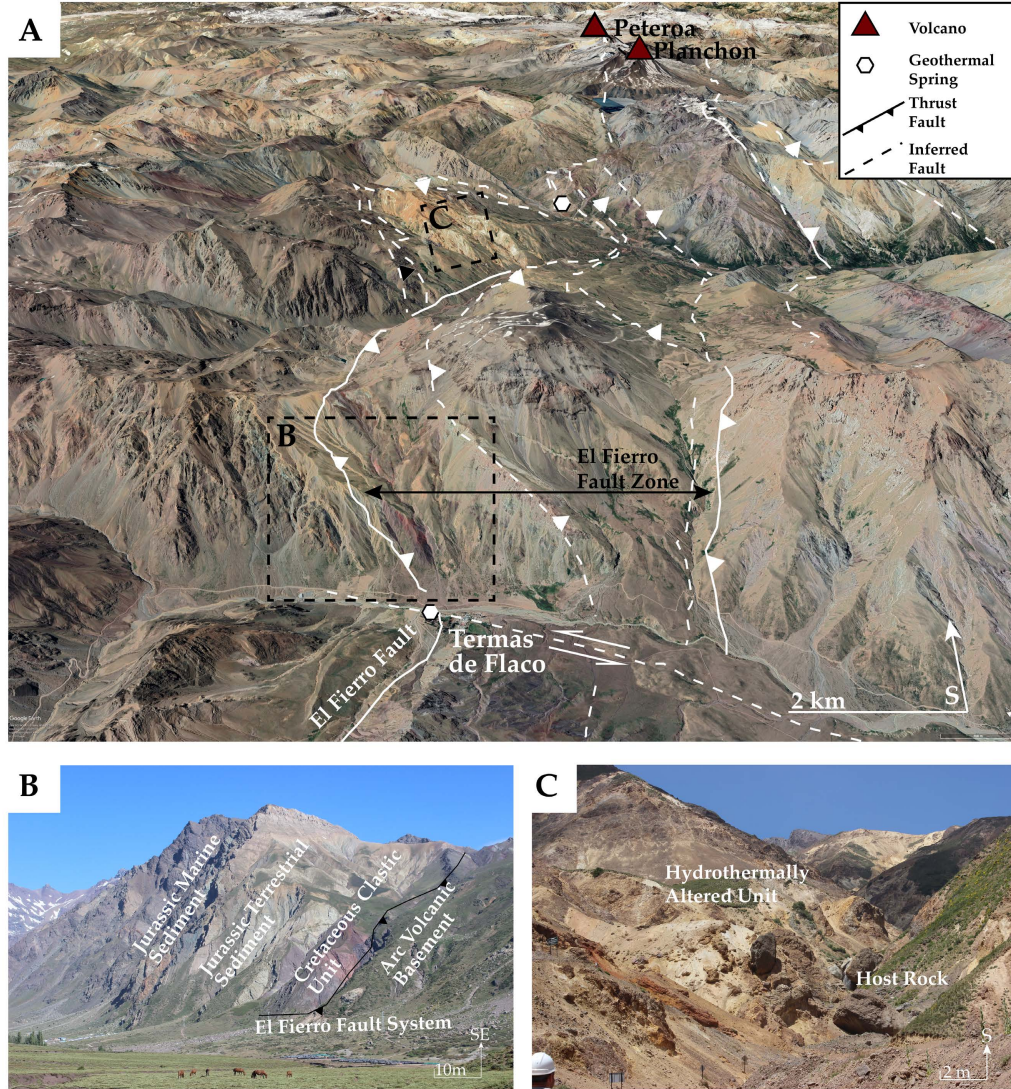
of thermal activity near Tinguiririca include high elevation fumaroles and lowland chloric springs, discharges of sulfuric rich mud pools and steam heated waters (Benavente et al., 2016; Pavez et al., 2016). The geochemical signatures of these springs and fumaroles suggest that they are sourced from a hydrothermal reservoir at 2-6 km depth and at temperatures of 230-250°C, that is recharged by shallow meteoric aquifers but that also bears trace elements of a deeper magmatic system (Aravena et al., 2016; Benavente et al., 2016; Pavez et al., 2016). A major signature of this system is the Termas de Flaco geothermal outflow spring (Figure 2B), which is commercially exploited. To the south, the Planchón-Peteroa volcanic complex is a series of Pleistocene - Holocene stratovolcanoes with five volcanic centers. Their activity progressed from earliest stage basaltic lavas to bimodal basaltic-andesitic and dacitic magmas extruded in subplinian explosions (Stern et al., 2007). Similar to Tinguiririca, fumarolic discharge occurs proximal to the Planchón edifice, with chemical signatures of a hydrothermal system recharged by meteoric waters, that also bear traces of He derived from a deep hydro-magmatic fluid source (Benavente et al., 2016). An episode of stratovolcanic eruption accompanied by ash discharge occurred between February - June 2011, placing Planchón-Peteroa on yellow alert eruption warning. It has since experienced sporadic events of degassing, water-vapor expulsion and shallow seismic tremors, the most notable events of which are an Mw 4 seismic event that occurred 4 - 7km beneath the summit on July 8th, 2017, and an explosive ash emission in September 2018 (Nover, 2005; Global-Volcanism-Program, 2019).

2.2 Faulting, kinematics and hydrothermal alteration

The largest structural feature in the study area is a segment of the 200km long El Fierro Fault System (EFFS), a sub-vertical, reverse drag thrust fault that formed during the late-Eocene to Oligocene. Thrust faulting deformation initiated when thickening of the lower crust was assisted by magmatic softening, and arc rocks were subsequently displaced eastward and uplifted along this fault (Charrier et al., 2002; Gow & Walshe, 2005). This was followed by inversion and thrusting of the Oligocene-Miocene volcanic sediments over the Mesozoic formations during the mid-Miocene to Pliocene (Charrier et al., 2002; Gow & Walshe, 2005). Kinematic analysis of this fault system suggests that, while the dominant structure formed from reverse faulting, the current deformation mechanism is dextral strike slip under regional transpression (Giambiagi et al., 2019). Outcropping fault strands of the EFFS show distinct alignment with volcanic and geothermic features in the area (Figure 3a). Additionally, significant hydrothermal alteration is seen in the Oligocene to Miocene volcanic and sedimentary rocks, spatially related to the hanging wall of the EFFS (Figure 3c). The alteration in this zone is of philic-argillic type with pervasive pyrite veinlets. The alteration appears to be strongly controlled by lithology, where the more fractured and permeable units exhibit stronger alteration. Additionally, we observe a supergene alteration, that produces oxidation and leaching of sulphides (i.e. pyrite), forming limonites (Jarosite > Goethite> hematite). This alteration is restricted to within the strands of the El Fierro fault, and the foot wall (Figure 3a & c).

Previous seismic tomography studies have inferred that the permeable damage zones of the EFFS act as channels for meteoric and magmatic derived fluids into the geothermal fields and outflow springs (Pavez et al., 2016). This has recently been debated by Giambiagi et al. (2019), who state that a blind NNE oriented strike-slip fault at 2.5km depth controls the migration of fluids, due to strong directional permeability that occurs at the fault intersection with the strands of the EFFS. This blind fault acts to localize hydrothermal fluid circulation, which in turn increases the fault's probability of failure due to increased pore fluid pressures along the fault plane. This became apparent when a seismic swarm in 2010 took place highlighting the geometry of this blind fault plane, whereas the EFFS remained relatively aseismic (Lira, 2011). The 2010 seismic swarm is considered to be related to local stress redistribution from the 6.5Mw sinistral strike-slip earthquake (Figure 2b). From this event, along with local paleostress analysis in the Tinguiririca valley, an ESE oriented sinistral strike slip regime was found to dominate this region (Giambiagi et al., 2019).

Figure 3. A) Satellite image of the field area looking SSE, displaying the primary features of interest, the trace of El Fierro thrust fault system is taken from Pavez et al. (2016), and inferred sinistral strike-slip faults (potential ATF) from Giambiagi et al. (2019). The larger and smaller black frames in a indicate the locations of B and C respectively. B) Photo showing the high angled El Fierro fault plane creating the unconformity between the Jurassic sediments and Quaternary volcaniclastics. C) Photo showing hydrothermally altered, Oligocene-Miocene volcanic host rock.

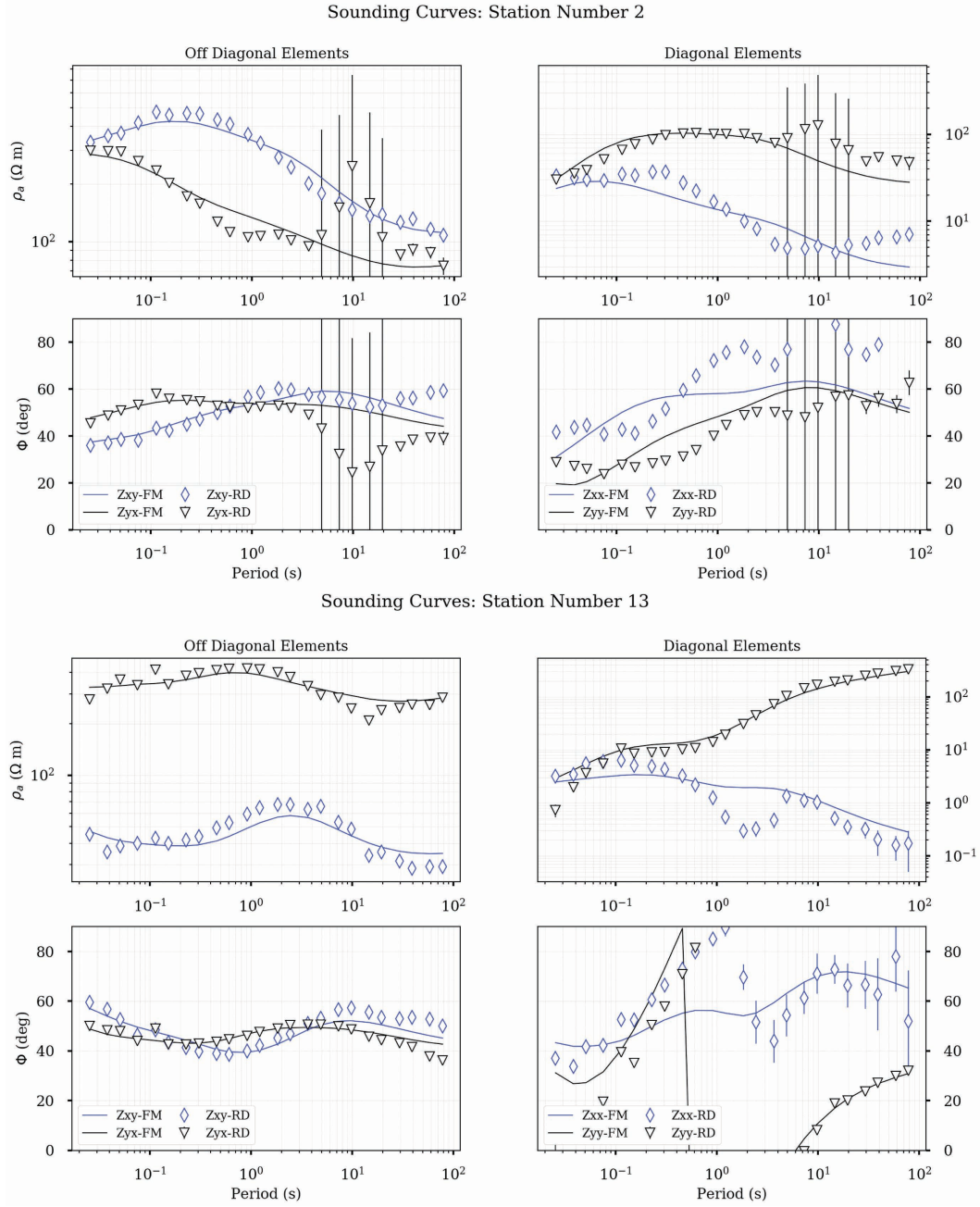## 3 Geophysical Data Acquisition and Processing

Magnetotellurics (MT) is a geophysical method that uses naturally occurring electromagnetic fields to estimate the electrical conductivity structure of the subsurface (Simpson & Bahr, 2005; Chave & Jones, 2012). Coupled with MT, precise hypocentre locations in seismically-active areas can detect the presence, geometry and distribution of faults that may interact with crustal fluids (Ingham et al., 2009; Wannamaker et al., 2009; Legrand et al., 2011; Held et al., 2016). For these reasons, this study combines seismic hypocenters manually picked form the seismic array with a 3D model derived from magnetotelluric data.

3.1 Magnetotelluric Survey, Data Processing and Inversion

In magnetotellurics, naturally occurring electromagnetic fields incident on the Earth's surface are passively and independently measured as a continuous time series of two horizontal electric components, E_x, E_y, and two horizontal magnetic components, H_x and H_y. When converted into the frequency domain, the response of the electric current to a varying magnetic field is quantified as the complex impedance tensor as a function of frequency, Z_ω. These impedance responses are then used to model conductivity variations of the Earth's subsurface through the relation $E = ZH$ (Simpson & Bahr, 2005).

The field campaign involved the collection of 26 broadband induction coil MT sites with approximately 5km spacing in a 40km^2 field area (Figure 2B). At all MT stations, the North-South (x) and East-West components (y) of the electric and magnetic fields were independently measured, as well as a vertical component of the magnetic field. MT data were collected using Metronix ADU-07e systems equipped with MFS-06e or MFS-07e coils. The experiment sampled at 1024Hz for an initial 30 minutes, after which data was collected at a 128Hz sampling rate for 48 hours. As the features of interest in this study are concentrated in the eastern limits of the surveyed area, namely the EFFS and the along-strike Tinguiririca and Planchón-Peteroa volcanic complexes, the MT grid has a dense NS oriented transect in this sector, while the three EW transects act as regional controls. The data processing method used was the Bounded Influence Remote Referencing (BIRRP) program (Chave & Thomson, 2003; Chave, 2004). This well-established MT data processing algorithm uses statistically robust techniques such and remote referencing to yield the impedance responses at selected frequencies. Of the completed 26 sites, data from 3 stations have been discarded due to irreparably poor data quality attributed to cultural and natural noise contamination, such as electric dipole interference or current channeling respectively. Some datasets also feature Galvanic Distortion, which is caused by near-surface conductivity heterogeneities at the measurement site (Bibby et al., 2005). The period bands affected by high levels of artificial noise were masked by assigning high error values to the data points in order to reduce the impact of noisy data on the inversion results. The 3D inversion of the 23 station MT grid was performed with a quasi-Newton optimization method that minimizes the data misfit and Tikhonov-type regularization parameter (D. B. Avdeev, 2005; D. Avdeev & Avdeeva, 2009). The algorithm uses joint inversion methods to correct for galvanic distortion inherent in the data. The distortion correction multiplies the frequency-independent, real valued distortion matrix, C, to the complex, frequency-dependent impedance tensor in the form $Z_{obs} = CZ$ (Avdeeva et al., 2015).

The initial mesh comprised 80x80x30 cells, with cell dimensions of 1000m x 1000m x 100m that was increased by a factor 1.1 times the vertical cell length per layer. The inversion was conducted with an error floor of 5% for the impedance datasets, and a large regularization parameter that was reduced by one order of magnitude per inversion run. Homogeneous meshes with initial conductivities 100, 500 and 1000Ωm were used as starting models to conduct full inversions, and to produce a layered models based on the 1D inversion of the average of the dataset. The layered models all resulted in a mesh of an overall 500Ωm resistivity with a 50 - 100Ωm layer between 8 - 14km. This layered model was the starting mesh for the final model that was selected for further analysis. The final preferred model,

Figure 4. Magnetotelluric apparent resistivity and phase results for all impedance tensor components (Z_{xx}, Z_{xy}, Z_{yx} and Z_{yy}) as a function of Period (s) for stations 2 and 13. Within each graph, black inverted triangles and blue diamonds show the data and black and blue lines (FM) are the responses of our preferred model.
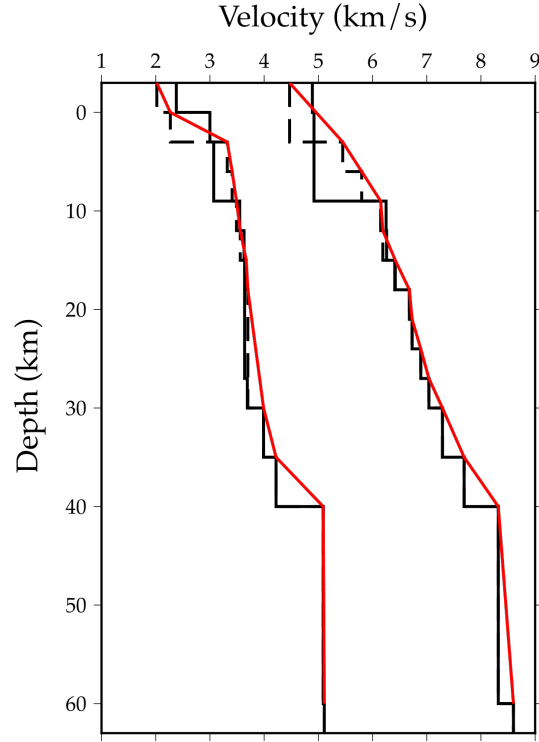
which was obtained after 800 iterations, reduced the RMS from a value of 9 to 1.55. The conductivity structure that emerged in this model was also observed in models with other initial conductivities, which supports the robustness of the result. While the RMS is a good overall measure of the fit between the synthetic model and the real data, we also examine the closeness between the sounding curves of both datasets for individual stations (Miensopust et al., 2013). An example of the real data and model fit for stations 2 and 13 is provided in Figure 4, which include all impedance components (Z_{xx}, Z_{xy}, Z_{yx} and Z_{yy}). The results for station 2 show that the model and real datasets fit well, apparent as the synthetic model data and real data (labelled FM and RD on Figure 4 respectively) closely match across all period bands. The Z_{yx} component Station 2 (Figure 4A) shows some scatter around the 3 - 12s period band, but this does not affect the synthetic data due to the high errors assigned to these data points. The off-diagonal components of station 13 exhibit some Galvanic Distortion, apparent as Z_{yx} is shifted to an apparent resistivity above Z_{xy} by approximately one decade across all period bands. As discussed, this type of Galvanic distortion is accounted for in the joint inversion by the distortion tensor, and the synthetic model (FM, Figure 4B) data and real data (RD, Figure 4B) are fit well despite the distortion, as was the case for all Galvanically distorted datasets (see Supplementary Material for the real and model data fits for each station). Furthermore, sensitivity tests were carried out to verify the robustness of each conductive structure within the model (see Supplementary Information on these techniques).

3.2 Seismic Survey and Hypocenter Location Processing

A network of 12 broadband seismometers (6 Güralp CMG-6TDs and 6 Güralp CMG-3ESPCDs) were deployed from April 2017 until December 2018 (Hammond et al., 2017). Average inter-stations spacing was approximately 15 km, mimicking the MT stations distribution (Figure 2B). Hypocenters were automatically detected using the QuakeMigrate software. QMigrate scans the seismic trace at each station by determining a STA/LTA onset function with high values representing phase arrivals (Drew et al., 2013). The onset functions are then backpropagated in a travel-time grid determining a 4D function representing the combined onsets spatially and through time, termed coalescence. The maximum coalescence for each time interval is then extracted, and when this value exceeds a user defined threshold value, an event is triggered. A marginal window, representing the expected model error, is taken about each event with the 4D coalescence stacked in the temporal domain to give a probability map of the earthquake location. Events are then filtered using the local- and global-gaussian error ellipses, with events with a large global-gaussian to local-gaussian rejected as they represent false triggers. This procedure outputs an automated catalogue of earthquake locations, expected location uncertainties and phase arrivals. The resulting QuakeMigrate catalogue was visually inspected afterwards, to manually update P- and S-wave arrivals. These revised travel-time picks were then used to estimate hypocenters using HYPOINVERSE-2000 (Klein, 2002).

Earthquake locations are sensitive to the velocity model used. We initially located a portion of our earthquakes catalogue using the velocity model calculated for the Southern Andes Volcanic Zone by Sielfeld et al. (2019). From this we obtained 205 hypocenters, with horizontal error < 2km and vertical error < 5km, azimuthal gap 87 - 336° and residuals (RMS) of 0.01s - 0.29s. We then updated the model by iteratively inverting for the resulting locations and the initial 1-D velocity model using VELEST (Kissling et al., 1994). VELEST allowed us to iteratively improve the RMS-misfit between calculated and observed travel times of each solution through updating the velocity model and relocating the earthquakes. 5 different a-priori models were tested including constant velocity models and CRUST1.0. All models showed similar trends, requiring a low velocity shallow crust, but the modified 1D velocity model of Sielfeld et al. (2019) proved to be the best model with the lowest RMS-misfit. The final model used in this study is shown in Figure 5. The homogeneous velocity layers in our best solution model were converted into gradient velocity layers, to reduce the depth-clustering effect that sharp velocity discontinuities have on hypocenters

Figure 5. P- and S-waves velocity models. The black solid lines represent the model of Sielfeld et al. (2019), the red solid lines show the velocity model updated for this study, and the black dashed lines represent the gradient velocity laters that reduce the sharp discontinuity that occurs at 10km depth

location due to seismic rays being modelled as refracted from discontinuities instead of realistic down-going rays with spread emergence angles (Klein, 2002). The final seismicity catalogue consists of 624 earthquakes with mean errors of 0.69km with 0.24 standard deviation horizontally and 1.21km and 0.74 standard deviation vertically.

4 Correlating conductivity anomalies with seismic features

The resolution of conductivity anomalies to be discussed have been validated with a series of robustness tests.The supplementary material presents details on these techniques, and specific tests will be referred to where required. All anomalies are shown to be required to fit the model to the collected dataset, however on notable region if low resolution is below the anomaly Con. 1 (Figure 6 & 7, sensitivity tests 3 & 4). The mean errors in the final hypocenters catalogue are 0.69km with 0.24 standard deviation horizontally and 1.21km and 0.74 standard deviation vertically.
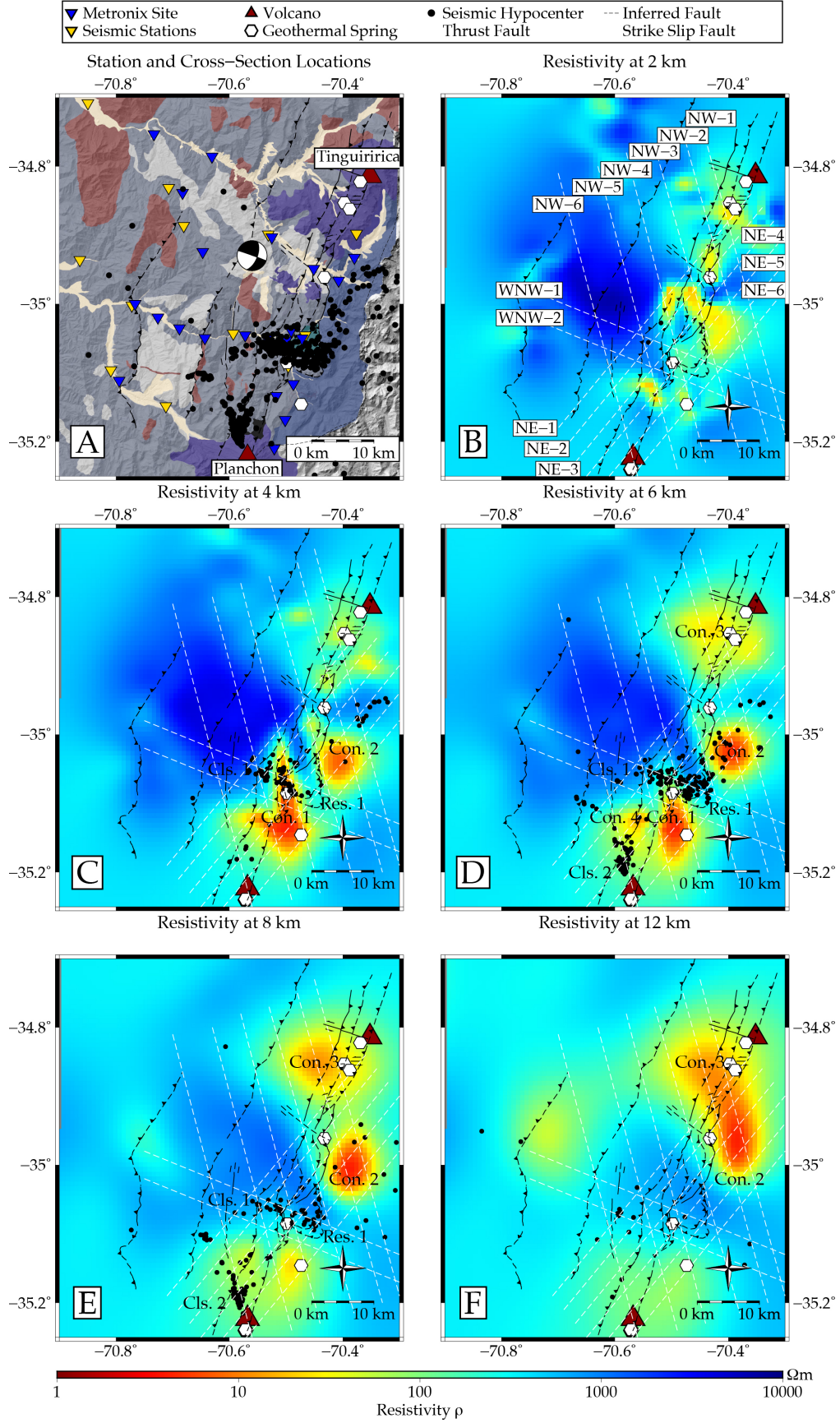
Two distinctive resistivity domains can be distinguished in the study area: an eastern domain of low resistivity (<50 Ωm, sensitivity test 16) and high concentration of hypocenters following the trace of the El Fierro fault system, and a western domain of high resistivity (values between 500 - 10,000 Ωm, sensitivity tests 8 & 9) and low seismicity (Figures 6 & 7). These two domains are best shown in cross-sections WNW-1 and WNW-2 (Figure 7), both of which are perpendicular to the general trend of the resistivity contrast and trace of the El Fierro fault system.

The eastern domain of low resistivity is segmented in the north-south orientation, populated by four distinct conductors (Con. 1, Con. 2, Con. 3 and Con. 4, sensitivity tests 1, 6, 7, 8, 12 & 13) and 2 main seismic clusters (Cls. 1 and Cls. 2) (Figure 6 & 7). The conductor Con. 1 occurs NE of the Planchón-Peteroa volcanoes at a depth of 4 - 8km and correlates with the seismic cluster Cls. 1. At 6km (Figure 6D) Con. 1 is at its maximum lateral extent. The seismic cluster (Cls. 1) follows a WNW oriented trend that aligns with an abrupt boundary between Con. 1 and a WNW oriented resistive corridor (conductivity ranges 500 - 1,000Ωm), Res. 1 (sensitivity tests 10 & 11).
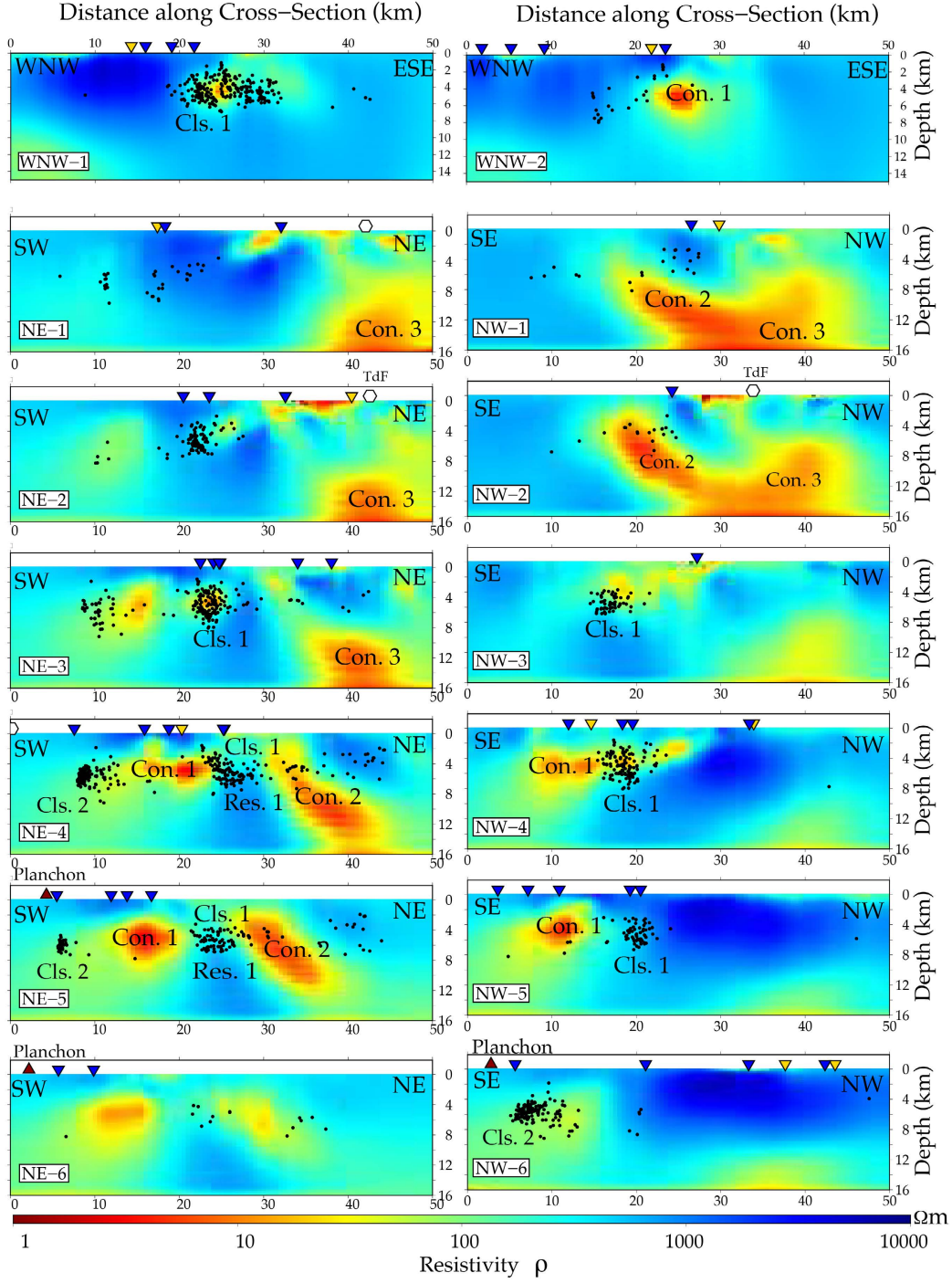
The seismic cluster Cls. 2 also occurs at a boundary between a conductive anomaly (Con. 4) and more resistive region. The most southeastern cross-sections, NE-5 & NE-6 (Figure 6) show the progressive disappearance of these features, as conductors Con.1 and 2 begin to diminish in strength towards the SW, and seismic clusters dissipate in NE-5, until there is little distinguishable conductive or seismogenic structure in NE-6. This is also a likely result of the model region extending outside the seismic and MT array.

It is apparent that there is a south to northward increase in high conductivity anomalies between 8 - 12km depth (Figure 6 E& F, sensitivity tests 12 & 13), and an apparent connection between Con. 2 and Con. 3 at 12km (Figure 6E & F). A smaller conductor, Con. 2 (conductivity ranges 5 - 50Ωm) is present at 4km depths (sensitivity test 15), and connects to a deeper conductor, Con. 3, at 10km depth along an approximate north-eastern dip. As MT is has difficulty to resolve the exact dip of the conductive anomalies, unless a very dense, localized survey is conducted, this dip angle can only be estimated. The conductor Con. 3 also seems to be connected through minor conductive branches with the shallow conductor correlated with the Termas del Flaco geothermal spring (NE-1, NE-2, NW-1 and NW-2, Figure 6), a known outflow of the Tinguiririca geothermal fields (Aravena et al., 2016; Benavente et al., 2016; Pavez et al., 2016).

The seismic cluster Cls. 2 is predominantly focussed at 6 - 8km depths in a region of low to intermediate resistivity (10 - 50 Ωm, Con. 4 in Figure 6D-E, sensitivity test 18). The shape of this cluster is very similar to that of the contour of the conductive anomaly, suggesting a connection between the two (Figure 6D). Furthermore, all seismic hypocenters occur within a 0-8km depth range (see Figures 6 & 7) with some anomalously deeper seismic

Figure 6. A) hypocenters located from the local seismic survey, projected onto a the 12m resolution DEM of the field study area along with important geological features (see Figure 2 for feature refernces). B-F: 3D MT models plotted with seismic hypocentres at depths 2, 4, 6, 8, and 12km respectively, with seismicity projected within ±200m at each depth. The EFFS, volcanoes, and geothermal springs are projected onto each map to indicate their surface localities. A-F: White dashed lines indicate the location of the cross-sections provided in Figure 7.

Figure 7. A set of fourteen cross-sections of the MT inversion model between 0 - 16km's, with seismic hypocenters projected within +/-200m lateral distance from the transect location. Also projected are MT and seismic station locallitions (blue and red triangles respectively) that occur along the transects. See Figure 6 for profile locations. Conductive and seismic features described in the paper (Con. 1, Con. 2, Con. 3, Res.1, Cls.1 & Cls.2) are labelled.

events that occur at 15km depths beneath the Planchón-Peteroa volcanic complex (NW-6, Figure 7).

In summary, seismic and conductive anomalies appear correlated in Figures 6 and 7. Both high conductivity anomalies and seismogenic zones occur along the NNE oriented trend of the volcanic complexes and EFFS. There is also a prominent WNW oriented seismic cluster, Cls. 1, that occurs along an abrupt conductivity boundary (Con. 1 and Res. 1) of the same orientation, that emerges at 4km depths and is strongest at 6km depths. Below 8km, the region is aseismic, and a deeply rooted conductor (Con. 3) emerges beneath the Tinguiririca complex at 12km depth connected to a smaller conductive limb that shallows towards the south (Con. 2). Finally, a small seismic cluster (Cls. 2) shows coherent geometry and locality with a moderate conductor (Con. 4) at 6-8 km depths, slightly northwest of the Planchón-Peteroa edifices.

5 Discussion

The following discussion points address the observations presented in the previous section. It is noted that, while there is confidence in the spatial distribution of the conductors in the final MT model, there is some ambiguity as to the absolute conductivities of each feature. When a precise range of resistivity values for MT anomalies is defined, lithological properties of subsurface melt and crystalline mush in the Andean volcanic-arc setting can be resolved (Pommier, 2014), such as melt-fluid fractions (e.g. Díaz et al., 2015; Cordell et al., 2018) or melt viscosity and silica content (e.g. Comeau et al., 2016). However, this analysis is best conducted if specific resistivity values as well as local rheological properties (e.g. melt composition) are well constrained, and isothermal profiles or the depth extent of hydrothermal fluid circulation domains are known. Properties of fault zones can also be determined due to the electrically conductive properties of graphite that can form within the fault core (e.g. Held et al., 2016), however significant assumptions are required if the fault zone parameters, such as cementation factor, porosity, and clay content, are undefined. Due to the lack of these constraints local to the studied field area, resolving the lithological properties of conductive phases is beyond the scope of this study. This analysis will be performed when further constraints are provided by seismic dataset, using methods such as seismic tomography, evaluating shear-wave ratios, or comparing velocity models to resistivity profiles using the techniques described by Comeau et al. (2016). Interpretation of the integrated seismic hypocenter and MT model are thus focussed on discerning between melt or hydrothermal fluids, and their relationship to the seismic features that have been detected.

5.1 Role of the El Fierro Fault System

It is apparent that the conductive zones are located along the axis of the active volcanic chain (Figure 6B). This suggests that the conductors are likely reserves of fluid and/or hydrous melt related to the active volcanic arc. As mentioned in section 3, the Andean volcanic arc has an anomalously high geothermal gradient and high concentrations of magmatically sourced fluids (Benavente et al., 2016; Giambiagi et al., 2019), both characteristics of which are associated with high conductivity (Ramos, 2010; Turienzo et al., 2012). This correlation of conductive anomalies located along the axis of the volcanic are has been observed in multiple comparable MT studies conducted in the Southern and Central Andes (e.g. Díaz et al., 2015; Kapinos et al., 2015; Held et al., 2016).

This east-west divide is particularly apparent in cross-sections WNW-1 and WNW-2 (Figure 7), on which the dip of the El Fierro fault plane has been projected using structural data from previous studies of this fault system (Godoy et al., 1999; Giambiagi et al., 2019). It is apparent that the seismicity cluster Cls. 1 and conductive anomaly Con. 1 are contained within the footwall of the EFFS. It is here considered that the fault plane acts as a barrier to cross-fault fluid migration, hence all magmatic-derived hydrothermal fluid circulation

and associated seismogenic processes occur east of the fault trace. This is supported by the exhumed alteration zone that occurs on the footwall of exposed fault surface expression (Figures 3B and 4) and that all geothermal springs and fumaroles are found along eastern strands of the fault system (Pavez et al., 2016).

5.2 Brittle-Ductile Transition

There is a distinct seismic boundary at a depth of 9 - 10km, below which no seismicity is apparent in any cross-section with some exceptions beneath the Planchón-Peteroa complex (Figure 7). Such a seismic boundary was observed in the regional scale seismic survey conducted by Sielfeld et al. (2019) between latitudes 38 - 40°S. Their results show an upper-crustal concave seismic boundary that traverses the Andes. It is considered concave as the seismic depth limit is 40km at the plate margin, 20km at the fore-arc in Argentina, and 10-12km depth in the Principle Cordillera that is located between the margin and forearc (Lange et al., 2008; Legrand et al., 2011). It was established by Sielfeld et al. (2019) that this seismic boundary marks an approximate isotherm of 340°C, based on preceding global/borehole studies of quasi-plastic deformation in the crust (Suzuki et al., 2014), and delineates the brittle-ductile transition zone within the SVZ. The same interpretation of the seismic boundary used by Sielfeld et al. (2019) and other comparable MT studies conducted in the southern Andes (e.g. Held et al., 2016) will be applied to the hypocenter results we have observed. Therefore, the local seismic boundary at 9-10km depth in our area to be the brittle-ductile transition zone, which marks an approximate 340°C isotherm.

5.3 Hydrothermal fluids beneath the Planchón-Peteroa Volcano

The seismic cluster Cls. 2 occurs at 4 - 8km depths beneath Planchón-Peteroa (Figure 7, NE-4, NE-5 & NW-4), and is concurrent with a moderate conductivity anomaly of 10 - 50Ωm, that appears to have some spatial coherence to Con. 1. Furthermore, as there is low resolution in the MT model beneath Con. 1, and as this conductor occurs at the edge of the MT array, it is possible that a more conductive medium occurs below or south of Con. 1 & 4 that is not resolved by the model. With this ambiguity in mind, the following rationale provides supportive evidence that Con. 1 & 4 is likely hydrothermal fluids with some magmatic source. The precise location of this magmatic source of these fluids remains unknown due to the non-robust regions of the model below and south of Con. 1 and & 4.

The source of Con. 1 and Con. 4 conductivity anomalies is favoured to be the migration of fluids rather than magma or crystalline mush, based on previous studies of the Planchón-Peteroa volcanic activity that has occurred since 2011. It was determined by Aguilera et al. (2016) that the main phreatic eruption episode was driven by the release of deep magmatic gases and volatiles from a shallow hydrothermal-magmatic reservoir. Tephra fall and vapour emissions contained no juveline magmatic constituents and was mainly of hydrothermal origin. These volcanics products did, however, bear traces of deep oxidized magmatic fluids from a highly degassed (old) magmatic body, likely of dacitic or basaltic composition (Tassi et al., 2016). These results are supported by Benavente et al. (2016), who detected minor He signatures of a deep magmatic body within a dominantly hydrothermal regime below the volcano. It is therefore likely that the conductivity of Con. 1 is largely sourced from the hydrothermal system attested to by these studies. Furthermore, as the geothermal regime at depths between 0 - 8km is colder than 340°C (see previous subsection), and as the hydrothermal systems local to this region are established to be at approximately 250°C (Benavente et al., 2016), Con. 1 and Con. 4 are within the correct depth and temperature range to source the expression of these fluids.

Finally, an InSAR study conducted by Pritchard et al. (2013) regarded the subsidence of the Southern Andean volcanoes after the 2010 Mw 8.10 Maule earthquake. Results showed that the majority of ground deformation, which signify the release of fluids from the subvolcanic hydrothermal systems, do not occur directly beneath the volcano edifice, but

extend outwards from the main caldera. This study provides supportive evidence that the main fluid reservoirs local to individual volcanoes show some lateral displacement from the volcano, as is the case for the proximity of Con. 1 and the Planchón-Peteroa complex.

Having attributed the conductor Con. 1 to a resource of hydrothermal fluids, it is a likely explanation that the seismic cluster, Cls. 2, is induced by fluid migration or degassification of the volcano rather than the migration of magmatic material. This is supported by the recent effusive eruptions that have characterized the volcano, which are largely of ash and vapour emissions (section 2.1), its spatial association to the fluidized (conductive) zones proximal to the volcano (Con. 1 and Con. 4), and the evidence provided by Benavente et al. (2016) & Tassi et al. (2016) that the pluton within Planchón-Peteroa is cool and mature. Distinguishing whether the cluster is sourced from a redistribution of tectonic stress requires further spatial, temporal and kinematic analysis with the seismic study. However, as the presence of fluids commonly contribute to seismogenic processes due to the reduction of effective stress local to the faulted feature (Cox, 2005, 2016), it is reasonable to expect that fluids are present within this cluster. Therefore, this seismic cluster is considered a fluid injection point, where episodic seismic release enhances fluid migration occurring within the volcano.

5.4 Deeply rooted Conductor beneath Tinguiririca

Care must be taken interpreting the deeper feature, Con. 3, beneath Tinguiririca as this deeper structure is beyond the lateral boundaries of the MT station deployment. However, as magnetotelluric measurements are capable of increased lateral coverage with increasing depth, and as this feature and its connectivity to the conductive feature Con. 2 is shown to be robust within the inversion model (sensitivity tests 12, 13 & 15), interpretation is briefly explored.

Con. 3 is located in the vicinity of the Tinguiririca volcanic complex and is spatially associated with geothermal outflow springs at Termas del Flaco (refer to section 2.1) (Clavero et al., 2011; Pritchard et al., 2013; Aravena et al., 2016; Pavez et al., 2016). Its connectivity to the conductive limb, Con. 2, suggests that the shallower conductor is also a component of the active hydrothermal system that has been detected in this area. As trace elements of magmatic sources have been measured in the fumaroles and outflow springs associated with the Tinguiririca geothermal fields (Benavente et al., 2016), it is possible that these conductors comprise of both magmatic material and hydrothermal fluids. This is difficult to distinguish with the MT results alone, however some rationale can be applied to discern the composition of these conductive anomalies.

Considering the dimensions and shallowness of Con. 2, (it extends from 0-8km depths and has a volume of approximately 5km^3), it is unlikely that this is magma or crystalline mush as some volcanic orogenesis would be situated above the conductive feature (Figure 6C-E), as is observed in comparable studies based in the Andes (e.g. Comeau et al., 2016; Cordell et al., 2018). Similar to Planchón-Peteroa, the temperature of the hydrothermal system is estimated to be 250°C between 2 - 6km depths (Benavente et al., 2016), which suggests a mid-temperature, hydrothermal system is dominant at this depth range. This is supported by the correlating locality of the alteration zone that outcrops at the footwall of the El Fierro fault (Figure 6A), which occurs directly above the conductor Con. 2 (Figure 6B). This suggests that fluidized zones have historically migrated towards the surface at this locality. It is possible that the Con. 2 anomaly is not generated by hydrothermal fluids but by the conductive lithological phases of hydrothermally altered material. This does not conflict with the interpretation that Con. 2 is an ascending limb of the hydrothermal system, but it implies that this circulation is extinct.

The deeper conductor Con. 3 is a valid contender as a magmatic reservoir, considering its depth extent (8-16km) and location directly beneath the Tinguiririca volcanic complex (Figure 6E-F). It was established by Pavez et al. (2016) that a magmatic body exists 8 -

12km beneath the Tinguirirca volcanic edifice, which was determined to be a major source for fluid upflow zones that manifest between 2 - 6km beneath the surface. The modelled MT results support this scenario, therefore it is interpreted that Con. 2 is the signature of zones of hydrothermal fluids migrating to the surface through brittle lithologies, and that Con. 3 is generated by crystalline mush or a magmatic body that is a major source of these fluids, as well as the geochemical traces of magma that have been detected in the vicinity of this volcano (Benavente et al., 2016; Pavez et al., 2016). This model has also been proposed in other districts of the Andes, where a deep (10 - 14km) conductor beneath a volcanic edifice is considered a magma reservoir (Díaz et al., 2015; Comeau et al., 2016), and is the source for hydrothermal reservoirs that circulate in the shallow crust and generate shallower conductive anomalies (Díaz et al., 2015).
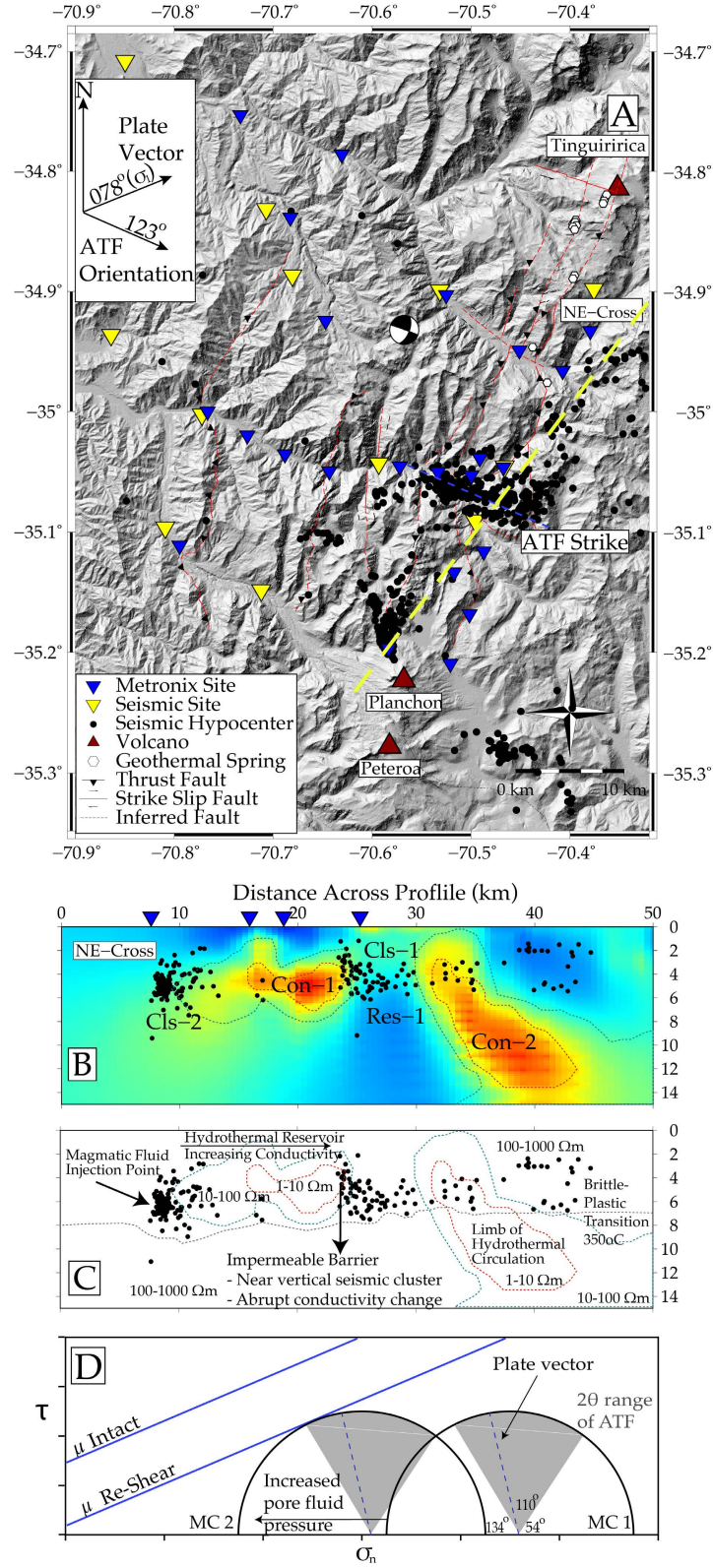
6 Novel insights into ATF and Hydrothermal System interaction

Conductor Con. 1 and seismic cluster Cls. 1 are focused between 4 - 8 km depths and both reach a peak strength at 6km depth (Figure 6D). The seismic cluster Cls. 1 has a distinct WNW orientation of approximately 10km length. This is interpreted to be an example of an active Andean Transverse Fault (ATF), as it is similar to others observed in different localities across the Andes (Chernicoff et al., 2002; Lara et al., 2004; Cembrano & Lara, 2009; Sielfeld et al., 2016, 2019; Stanton-Yonge et al., 2016; Roquer et al., 2017; Wrage et al., 2017). This cluster has a WNW oriented strike (Figure 8A), consistent with the interpretation of this boundary as an ATF. As discussed in section 1.1, these structures are considered reactivated pre-Andean fault planes, which exert a fundamental control in the location and development of volcanic complexes. They are enigmatic as they demonstrate seismic activity despite their unfavourable orientation with respect to the regional stress field (Cembrano & Moreno, 1994; Yáñez et al., 1998; Chernicoff et al., 2002; Sielfeld et al., 2019; Piquer et al., 2019). The seismicity of Cls. 1 does not extend to the surface, nor is there any surface expression of the structure, which supports the hypothesis that the ATF domain is contained within the basement lithology and that they are of Pre-Andean origin (Cembrano & Lara, 2009).

Recent insights from isotope geochemistry show that the geochemical signatures of water emerged from ATF have high degrees of crustal contamination (Tardani et al., 2016), signatures of magmatic vapourization of cold water recharge (Sánchez et al., 2013), and that the waters have a longer crustal residence time in the ATF domain relative to other major NNE trending fault systems (Wrage et al., 2017). Structural and mineralogical analyses of the faults have shown that fluid over-pressures between >85 - 98% of lithostatic stress can be required to nucleate seismic failure. It is therefore likely that fluid migration through these systems is required for their seismic activity, due to their oblique orientation to the prevailing stress field. Thus, these fault systems likely host hydrothermal reservoirs due to the entrapment of fluids during interseismic periods (Roquer et al., 2017). Finally, the ATF are characterized by multiple fault cores, and dense vein networks within a wide damage zone and therefore prevent cross-fault fluid flow due to their low permeability (Lara et al., 2004; Pérez-Flores et al., 2016).

The occurrence of seismogenic features at abrupt conductive boundaries has been observed in comparable MT and seismic studies conducted along the San Andreas Fault, Taupo Volcanic Zone and an intraplate setting in central Botswana (e.g. Becken et al., 2011; Ingham et al., 2009; Moorkamp et al., 2019). These studies suggest that earthquakes tend to occur adjacent to zones of high conductivity, either at the boundaries or within the regions of the neighbouring resistive rock. This is due to the migration of fluids into a permeable, mechanically weak zone (characterized by low resistivity) adjacent to a less permeable, mechanically strong zone (characterized by high resistivity). This causes the accumulation of high fluid pressures and subsequent brittle rock failure (Cox, 2005; Becken et al., 2011). This process can occur in fault zones, where impermeable fault cores prevent cross-fault fluid flow thus increase local fluid pressures, while the dense fracture mesh parallel to the

Figure 8. All manually picked seismic hypocenters from the local seismic survey, projected onto a the 12.5m resolution DEM of the field study area. The Teno earthquake moment tensor, geothermal springs, Holocene volcano locations and associated units, station locations and El Fierro fault zone are also shown. B) NE-oriented cross-section of the MT model with seismic hypocenters projected within a 200m lateral range of the cross section location; C) Schematic interpretation of the cross-section in panel B. D) a theoretical Mohr circle diagram illustrating the failure criterion envelopes for different stress regimes for fault re-shear, and the effect of pore fluid pressures on equivalent stress scenarios, each circle is marked as MC1 - 2. Greyed area represents range of quaternary stress orientations from Giambiagi et al. (2019).

fault core are highly permeable and enhance fault-parallel fluid flow (e.g. Sibson, 1967; J. Rowland & Sibson, 2004; Hoffmann-Rothe et al., 2004; D. R. Faulkner et al., 2010).

Furthermore, the predominance of seismicity at abrupt conductivity contrasts suggests that fluid accumulation can locally trigger reactivation of pre-existing ATF structures. It is interpreted that the smaller seismic cluster that resides beneath the Planchón-Peteroa system (Cls. 2) is a channel for volcanically sourced fluids that accumulate in a hydrothermal reservoir north of the complex. This reservoir is the source of the anomaly Con. 1, which increases in conductivity northwards until it reaches a maximum at the conductive boundary and seismic cloud, Cls. 1, apparent as the transition from the 75Ωm (yellow) to 5Ωm (red) region of the anomaly (Figure 8B-C).

We illustrate the state of stress using a Mohr-Coulomb failure diagram (Figure 8D), which is drawn on the assumption that the ATF are inherent pre-existing WNW pre-Andean structures with a strike of approximately 110° (estimated from the 2006 Mw 6.5 Teno earthquake focal mechanism (Ekström, 2012)) with no cohesive strength (Sibson, 1985). These faults activate as sinistral-strike slip and reverse under the current stress regime (Stanton-Yonge et al., 2016), which is evident from the 2004 Mw 6.5 focal mechanism (Figure 9A) and observations from similar ATF structures south of the studied area (Sielfeld et al., 2019). A simple Andersonian relationship is assumed (Anderson, 1951), where σ_2 is along the vertical axis and σ_1 and σ_3 are in a horizontal plane, and that σ_1 ranges between N65°E to N88°E, considering the possible scenarios of partially partitioned or non-partitioned regimes (Teyssier et al., 1995; Pérez-Flores et al., 2016). The angle between σ_1 and the fault plane is approximately between 58° to 35°, showing that it is not optimally oriented for reactivation. Therefore, ncreasing fluid pressure could induce reactivation of the fault by decreasing the effective normal stress. In the absence of local measurements of stress orientations, there is uncertainty as to whether the stress field includes strain partitioning across the transpressional plate margin (e.g. Tikoff & Teyssier, 1994; Teyssier et al., 1995) and/or mechanical interaction between faults across the volcanic arc (e.g. Stanton-Yonge et al., 2016). Future studies will be conducted using our seismic catalogue to determine fault plane solutions and conduct a kinematic analysis of fault-slip data, and thus constrain local stress orientations.

7 Final model of fault system control on hydrothermal reservoirs development

Figure 9A shows a 3D representation of the final model. It is interpreted that the resistive, seismogenic structure considered to be an ATF interacts with the deeply rooted conductor beneath Tinguiririca. We interpret the conductor Con. 2, to be the limb of a hydrothermal system sourced from a magmatic origin identified with the deeper conductor, Con. 3, as discussed in section 5.4. This limb appears to channel fluids towards the surface along the fault plane of the ATF, which dips towards the NE. Unlike the hydrothermal reservoir on the southern region (Con. 1), which results in overpressure and drives fault reactivation (section 6), the region surrounding this conductor Con. 2 shows no dense seismic clusters. We suggest that this conductor is a zone of permeable, saturated rock within which the pore fluid pressure is in excess of hydrostatic pressure. This can be inferred from the presence of significant geothermal outflow of deep-sourced fluids such as those found at Termas del Flaco, and contained in the geothermal fields associated with the Tinguiririca volcanic complex (Pritchard et al., 2013; Aravena et al., 2016; Benavente et al., 2016; Pavez et al., 2016; Giambiagi et al., 2019). Conversely, the Planchón-Peteroa reservoir has a resistive cap (Figure 7, NE-4, sensitivity test 3), suggesting that this reservoir is compartmentalized by the ATF and the resistive cap which leads to fluid overpressure. The presence of capping structures in the ATF domain have been previously hypothesized as a control on their rupture cycle (Roquer et al., 2017).

Figure 9. A) 3D presentation of the conductivity model at 4km depths along the horizontal plane, and cross-sections NE-4 and NW-2 (Figure 7) from 4-16km depths placed at accurate transect locations. Seismic hypocenters are shown along these planes to illustrate their distribution in 3D, with all seismicity projected onto the 4km horizontal plane to highlight the NW orientation of Cls. 1. Annotations highlight the interpretations discussed in sections 5 - 7, and the EFFS and volcanic complexes are projected at 0km depth to contextualize their locality at the surface; B) A schematic interpretation of the model results illustrates the hydro-volcanic system that is proposed for this upper crust of the surveyed area (Section 7)

While the placement of the Planchón-Peteroa hydrothermal reservoir appears constrained to the north by the discrete, blind ATF structure, it is also bound to the west by the El Fierro fault system (Figure 6A-D). It has been observed in different regions of the Andes that the intersection of major NNE thrust faults and ATF are hosts to giant ore-porphyry deposits (Figure 1) (e.g. Curewitz & Karson, 1997; Sillitoe, 1997; Chernicoff et al., 2002; Cox, 2005; J. V. Rowland & Simmons, 2012; Piquer et al., 2019). These points of intersection have also been deduced to impact geothermal reservoir development, (Sánchez et al., 2013; Pérez-Flores et al., 2017). Therefore, this study provides a site specific example of how the intersection of these major, margin-parallel thrust fault systems and Andean transverse faults are hosts to magmatically sourced geothermal reservoirs at 4 - 8km depths.

8 Conclusions

Results from this combined magnetotelluric and seismic study can be summarized with five distinct observations:

1. An eastern conductive and western resistive domain is correlated with a seismic boundary that occurs across all depths, and follows the trend of the volcanic arc and NNE striking El Fierro Fault system. This is interpreted to be the signature of magmatic sources beneath the volcanic arc. These are characterized by higher conductivity than the surrounding regions due to high temperatures and concentrations of volcanic derived fluids. It is also concluded that these conductive and seismic signatures are bound by the footwall of the El Fierro fault system, due to the low permeability fault cores that prevent cross-fault fluid migration.

2. A WNW striking seismogenic feature occurs on an abrupt electrical conductivity contrast between depths of 4 - 8km depths. We interpret this seismogenic feature to be a reactivated Andean Transverse Fault (ATF), and the electrically conductive domain to be a hydrothermal reservoir. We conclude that the impermeable fault core of the ATF prevents cross-fault fluid flow; therefore, the accumulation of fluids increases pore fluid pressures and induces fault reactivation despite its unfavourable orientation relative to the regional stress field.

3. A deep conductor beneath the Tinguiririca volcanic complex emerges at 8km depth and increases in volume and conductivity with increasing depth. It shows some connection to the surface with minor conductive branches that show spatial coherence with the major geothermal outflow spring Termas de Flaco. This high conductivity anomaly is considered a deep volcanic root that sources the geothermal springs and fumaroles observed at the base and edifice of the Tinguiririca volcanic complex, as well as the geothermal fields that have been thoroughly prospected in this area.

4. There is a minor seismic cluster and conductor beneath the Planchón-Peteroa volcanic complex that is highly concentrated at 8km depths. These volcanoes have been intermittently on yellow- alert for ash emission and degassing events since 2011 suggesting this seismicity is related to the release of volcanic derived fluids and volatiles into the shallower crust, recharging the hydrothermal reservoir above.

5. There is a distinct aseismic boundary at 8-10km depths, below which there is no seismicity. This is considered the brittle-ductile transition zone, and a definitive 340°C isotherm that is observed across the Andean volcanic margin.

This combined seismic and magnetotelluric study is the first in the vicinity of an ATF structure, showing how they interact with local volcanic and hydrothermal systems. Due to the spatial coherency of very distinct conductive anomalies, attributed to hydrothermal

fluids, it is proposed that these faults fail despite their misorientation to the regional stress field due to the influence of pore fluid pressures acting on the fault plane. The results also reveal how the architectural relationship of the ATF and NNE-striking, margin parallel fault systems exert significant control on the spatial development of hydrothermal reservoirs in the Andean Southern Volcanic Zone.

Acknowledgments

References

Acocella, V., Gioncada, A., Omarini, R., Riller, U., Mazzuoli, R., & Vezzoli, L. (2011). Tectonomagmatic characteristics of the back?arc portion of the calama?olacapato?el toro fault zone, central andes [Journal Article]. *Tectonics*, *30*(3).

Aguilera, F., Benavente, o., Gutiérrez, F., Romero, J., Saltori, O., González, R., ... Pizarro, M. (2016). Eruptive activity of planchón-peteroa volcano for period 2010-2011, southern andean volcanic zone, chile [Journal Article]. *Andean Geology*, *43*(2), 20-46.

Anderson, E. M. (1951). *The dynamics of faulting and dyke formation with applications to britain* [Book]. Hafner Pub. Co.

Angermann, D., Klotz, J., & Reigber, C. (1999). Space-geodetic estimation of the nazca-south america euler vector [Journal Article]. *Earth and Planetary Science Letters*, *171*(3), 329-334.

Aravena, D., Muñoz, M., Morata, D., Lahsen, A., Parada, M. a., & Dobson, P. (2016). Assessment of high enthalpy geothermal resources and promising areas of chile [Journal Article]. *Geothermics*, *59*, 1-13. Retrieved from http://www.sciencedirect.com/science/article/pii/S037565051500111X doi: https://doi.org/10.1016/j.geothermics.2015.09.001

Aron, F., Cembrano, J., Astudillo, F., Allmendinger, R. W., & Arancibia, G. (2015). Constructing forearc architecture over megathrust seismic cycles: Geological snapshots from the maule earthquake region, chile [Journal Article]. *Geological Society of America Bulletin*, *127*(3-4), 464-479.

Avdeev, D., & Avdeeva, A. (2009). 3d magnetotelluric inversion using a limited-memory quasi-newton optimization [Journal Article]. *GEOPHYSICS*, *74*(3), F45-F57. Retrieved from https://library.seg.org/doi/abs/10.1190/1.3114023 doi: 10.1190/1.3114023

Avdeev, D. B. (2005). Three-dimensional electromagnetic modelling and inversion from theory to application [Journal Article]. *Surveys in Geophysics*, *26*(6), 767-799. Retrieved from https://doi.org/10.1007/s10712-005-1836-x doi: 10.1007/s10712-005-1836-x

Avdeeva, A., Moorkamp, M., Avdeev, D., Jegen, M., & Miensopust, M. (2015). Three-dimensional inversion of magnetotelluric impedance tensor data and full distortion matrix [Journal Article]. *Geophysical Journal International*, *202*(1), 464-481. Retrieved from http://dx.doi.org/10.1093/gji/ggv144 doi: 10.1093/gji/ggv144

Becken, M., Ritter, O., Bedrosian, P. A., & Weckmann, U. (2011). Correlation between deep fluids, tremor and creep along the central san andreas fault [Journal Article]. *Nature*, *480*(7375), 87.

Benavente, O., Tassi, F., Reich, M., Aguilera, F., Capecchiacci, F., Gutiérrez, F., ... Rizzo, A. (2016). Chemical and isotopic features of cold and thermal fluids discharged in the southern volcanic zone between 32.5 s and 36 s: Insights into the physical and chemical processes controlling fluid geochemistry in geothermal systems of central chile [Journal Article]. *Chemical Geology*, *420*, 97-113.

Bertrand, E. A., Unsworth, M. J., Chiang, C., Chen, C., Chen, C., Wu, F. T., ... Hill, G. J. (2012). Magnetotelluric imaging beneath the taiwan orogen: An arc?continent collision [Journal Article]. *Journal of Geophysical Research: Solid Earth*, *117*(B1).

Bibby, H. M., Caldwell, T. G., & Brown, C. (2005). Determinable and non-determinable parameters of galvanic distortion in magnetotellurics [Journal Article]. *Geophysical Journal International*, *163*(3), 915-930. Retrieved from http://dx.doi.org/10.1111/j.1365-246X.2005.02779.x doi: 10.1111/j.1365-246X.2005.02779.x

Bonali, F., Tibaldi, A., Corazzato, C., Tormey, D., & Lara, L. (2013). Quantifying the effect of large earthquakes in promoting eruptions due to stress changes on magma pathway: the chile case [Journal Article]. *Tectonophysics*, *583*, 54-67.

Caine, J. S., Evans, J. P., & Forster, C. B. (1996). Fault zone architecture and permeability structure [Journal Article]. *Geology*, *24*(11), 1025-1028.

Cembrano, J., & Lara, L. (2009). The link between volcanism and tectonics in the southern volcanic zone of the chilean andes: A review [Journal Article].

Tectonophysics, *471*(1?2), 96-113. Retrieved from `http://www.sciencedirect.com/science/article/pii/S0040195109001310` doi: http://dx.doi.org/10.1016/j.tecto.2009.02.038

Cembrano, J., & Moreno, H. (1994). Geometría y naturaleza contrastante del volcanismo cuaternario entre los 38 s y 46 s: dominios compresionales y tensionales en un régimen transcurrente [Conference Proceedings]. In *Congreso geológico chileno* (p. 240-244).

Charrier, R., Baeza, O., Elgueta, S., Flynn, J., Gans, P., Kay, S., ... Zurita, E. (2002). Evidence for cenozoic extensional basin development and tectonic inversion south of the flat-slab segment, southern central andes, chile (33?36 sl) [Journal Article]. *Journal of South American Earth Sciences*, *15*(1), 117-139.

Charrier, R., Pinto, L., & Rodríguez, M. P. (2007). Tectonostratigraphic evolution of the andean orogen in chile [Journal Article]. *The Geology of Chile*, 21-114.

Charrier, R., Ramos, V. A., Tapia, F., & Sagripanti, L. (2014). Tectono-stratigraphic evolution of the andean orogen between 31 and 37s (chile and western argentina) [Journal Article]. *Geological Society, London, Special Publications*, *399*. Retrieved from `http://sp.lyellcollection.org/content/early/2014/08/20/SP399.20.abstract` doi: 10.1144/sp399.20

Chave, A. D. (2004). *Birrp: Bounded influence, remote reference processing* [Unpublished Work]. Woods Hole Oceanographic Institution.

Chave, A. D., & Jones, A. G. (2012). *The magnetotelluric method: Theory and practice* [Book]. Cambridge University Press.

Chave, A. D., & Thomson, D. J. (2003). A bounded influence regression estimator based on the statistics of the hat matrix [Journal Article]. *Journal of the Royal Statistical Society: Series C (Applied Statistics)*, *52*(3), 307-322.

Chernicoff, C. J., Richards, J. P., & Zappettini, E. O. (2002). Crustal lineament control on magmatism and mineralization in northwestern argentina: geological, geophysical, and remote sensing evidence [Journal Article]. *Ore Geology Reviews*, *21*(3), 127-155. Retrieved from `http://www.sciencedirect.com/science/article/pii/S0169136802000872` doi: https://doi.org/10.1016/S0169-1368(02)00087-2

Clavero, J., Pineda, G., Mayorga, C., Giavelli, A., Aguirre, I., Simmons, S., ... Polanco, E. (2011). Geological, geochemical, geophysical and first drilling data from tinguiririca geothermal area, central chile [Journal Article]. *Geothermal Resources Council Transactions*, *35*, 731-734.

Comeau, M. J., Unsworth, M. J., & Cordell, D. (2016). New constraints on the magma distribution and composition beneath volcán uturuncu and the southern bolivian altiplano from magnetotelluric data [Journal Article]. *Geosphere*, *12*(5), 1391-1421.

Cordell, D., Unsworth, M. J., & Díaz, D. (2018). Imaging the laguna del maule volcanic field, central chile using magnetotellurics: Evidence for crustal melt regions laterally-offset from surface vents and lava flows [Journal Article]. *Earth and Planetary Science Letters*, *488*, 168-180. Retrieved from `http://www.sciencedirect.com/science/article/pii/S0012821X18300177` doi: https://doi.org/10.1016/j.epsl.2018.01.007

Cox, S. (2005). Coupling between deformation, fluid pressures, and fluid flow in ore-producing hydrothermal systems at depth in the crust [Journal Article].

Cox, S. (2010). The application of failure mode diagrams for exploring the roles of fluid pressure and stress states in controlling styles of fracture?controlled permeability enhancement in faults and shear zones [Journal Article]. *Geofluids*, *10*(1?2), 217-233.

Cox, S. (2016). Injection-driven swarm seismicity and permeability enhancement: Implications for the dynamics of hydrothermal ore systems in high fluid-flux, overpressured faulting regimes?an invited paper [Journal Article]. *Economic Geology*, *111*(3), 559-587.

Curewitz, D., & Karson, J. A. (1997). Structural settings of hydrothermal outflow: Fracture permeability maintained by fault propagation and interaction [Journal Article]. *Journal of Volcanology and Geothermal Research*, *79*(3), 149-168. Retrieved from `http://www.sciencedirect.com/science/article/pii/S0377027397000279` doi: https://doi.org/10.1016/S0377-0273(97)00027-9

Díaz, D., Heise, W., & Zamudio, F. (2015). Three?dimensional resistivity image of the magmatic system beneath lastarria volcano and evidence for magmatic intrusion in the back arc (northern chile) [Journal Article]. *Geophysical Research Letters*, *42*(13), 5212-5218.

Drew, J., White, R. S., Tilmann, F., & Tarasewicz, J. (2013). Coalescence microseismic mapping [Journal Article]. *Geophysical Journal International*, *195*(3), 1773-1785.

Ekström, M. N. A. M. D., G. (2012). The global cmt project, 2004 - 2010 [Journal Article]. *https://www.globalcmt.org/CMTsearch.html*.

Farías, M., Comte, D., Charrier, R., Martinod, J., David, C., Tassara, A., ... Fock, A. (2010). Crustal?scale structural architecture in central chile based on seismicity and surface geology: Implications for andean mountain building [Journal Article]. *Tectonics*, *29*(3).

Faulkner, D., Mitchell, T., Jensen, E., & Cembrano, J. (2011). Scaling of fault damage zones with displacement and the implications for fault growth processes [Journal Article]. *Journal of Geophysical Research: Solid Earth*, *116*(B5).

Faulkner, D. R., Jackson, C. A. L., Lunn, R. J., Schlische, R. W., Shipton, Z. K., Wibberley, C. A. J., & Withjack, M. O. (2010). A review of recent developments concerning the structure, mechanics and fluid flow properties of fault zones [Journal Article]. *Journal of Structural Geology*, *32*(11), 1557-1575. Retrieved from `http://www.sciencedirect.com/science/article/pii/S019181411000101X` doi: https://doi.org/10.1016/j.jsg.2010.06.009

Giambiagi, L., álvarez, P., Spagnotto, S., Godoy, E., Lossada, A., Mescua, J., ... Suriano, J. (2019). Geomechanical model for a seismically active geothermal field: Insights from the tinguiririca volcanic-hydrothermal system [Journal Article]. *Geoscience Frontiers*. Retrieved from `http://www.sciencedirect.com/science/article/pii/S1674987119300623` doi: https://doi.org/10.1016/j.gsf.2019.02.006

Global-Volcanism-Program. (2019). *Planchon-peteroa (357040)* (Report). Smithsonian Institution.

Godoy, E., Yáñez, G., & Vera, E. (1999). Inversion of an oligocene volcano-tectonic basin and uplifting of its superimposed miocene magmatic arc in the chilean central andes: first seismic and gravity evidences [Journal Article]. *Tectonophysics*, *306*(2), 217-236.

Gow, P., & Walshe, J. (2005). The role of preexisting geologic architecture in the formation of giant porphyry-related cuau deposits: Examples from new guinea and chile [Journal Article]. *Economic Geology*, *100*(5), 819-833.

Hammond, J. O. S., Muela, A. S. D. L., Pearce, R. K., Marshall, N., Mitchell, T. M., & Cembrano, J. (2017). Teno valley seismic network [Journal Article]. *International Federation of Digital Seismograph Networks*. doi: Dataset/SeismicNetwork.doi:10.7914/SN/6A_2017

Hedenquist, J. W., & Lowenstern, J. B. (1994). The role of magmas in the formation of hydrothermal ore deposits [Journal Article]. *Nature*, *370*(6490), 519-527.

Held, S., Schill, E., Pavez, M., Díaz, D., Muñoz, G., Morata, D., & Kohl, T. (2016). Resistivity distribution from mid-crustal conductor to near-surface across the 1200 km long liquiñe-ofqui fault system, southern chile [Journal Article]. *Geophysical Journal International*, *207*(3), 1387-1400.

Hoffmann-Rothe, A., Ritter, O., & Janssen, C. (2004). Correlation of electrical conductivity and structural damage at a major strike-slip fault in northern chile [Journal Article]. *J. Geophys. Res*, *109*, B10101.

Ingham, M. R., Bibby, H. M., Heise, W., Jones, K. A., Cairns, P., Dravitzki, S., ... Ogawa, Y. (2009). A magnetotelluric study of mount ruapehu volcano, new zealand [Journal Article]. *Geophysical Journal International*, *179*(2), 887-904. Retrieved from `http://dx.doi.org/10.1111/j.1365-246X.2009.04317.x` doi: 10.1111/j.1365-246X.2009.04317.x

Kapinos, G., Montahaei, M., Meqbel, N., & Brasse, H. (2015). Three-dimensional electrical resistivity image of the south-central chilean subduction zone [Journal Article]. *Tectonophysics*.

Katz, H. (1971). Continental margin in chile–is tectonic style compressional or extensional? [Journal Article]. *AAPG Bulletin*, *55*(10), 1753-1758.

Kissling, E., Ellsworth, W., Eberhart?Phillips, D., & Kradolfer, U. (1994). Initial reference models in local earthquake tomography [Journal Article]. *Journal of Geophysical Research: Solid Earth*, *99*(B10), 19635-19646.

Klein, F. (2002). User's guide to hypoinverse-2000, a fortran program to solve for earthquake locations and magnitudes 4/2002 version [Journal Article]. *USGS, Open File Report 02-171 Version*, *1*, 123.

Lange, D., Cembrano, J., Rietbrock, A., Haberland, C., Dahm, T., & Bataille, K. (2008). First seismic record for intra-arc strike-slip tectonics along the liquiñe-ofqui fault zone at the obliquely convergent plate margin of the southern andes [Journal Article]. *Tectonophysics*, *455*(1-4), 14-24.

Lara, L., Naranjo, J., & Moreno, H. (2004). Rhyodacitic fissure eruption in southern andes (cordón caulle; 40.5 s) after the 1960 (mw: 9.5) chilean earthquake: a structural interpretation [Journal Article]. *Journal of Volcanology and Geothermal Research*, *138*(1-2), 127-138.

Legrand, D., Barrientos, S., Bataille, K., Cembrano, J., & Pavez, A. (2011). The fluid-driven tectonic swarm of aysen fjord, chile (2007) associated with two earthquakes (mw= 6.1 and mw= 6.2) within the liquiñe-ofqui fault zone [Journal Article]. *Continental Shelf Research*, *31*(3), 154-161.

Lira, E. S. (2011). Estudio de sismicidad, tomografía sísmica y modelo de física de rocas: potencial sistema geotermal asociado al complejo volcánico tinguiririca [Journal Article].

Melnick, D., & Echtler, H. P. (2006). Morphotectonic and geologic digital map compilations of the south-central andes (36?42 s) [Book Section]. In *The andes* (p. 565-568). Springer.

Micklethwaite, S., Sheldon, H. A., & Baker, T. (2010). Active fault and shear processes and their implications for mineral deposit formation and discovery [Journal Article]. *Journal of Structural Geology*, *32*(2), 151-165.

Miensopust, M. P., Jones, A. G., & Queralt, P. (2013). Magnetotelluric 3-d inversion- a review of two successful workshops on forward and inversion code testing and comparison [Journal Article]. *Geophysical Journal International*, *193*(3), 1216-1238. Retrieved from https://doi.org/10.1093/gji/ggt066 doi: 10.1093/gji/ggt066

Moorkamp, M., Fishwick, S., Walker, R. J., & Jones, A. G. (2019). Geophysical evidence for crustal and mantle weak zones controlling intra-plate seismicity?the 2017 botswana earthquake sequence [Journal Article]. *Earth and Planetary Science Letters*, *506*, 175-183.

Mpodozis, C., Ramos, V., Ericksen, G., Canas Pinochet, M., & Reinemund, J. (1989). Geology of the andes and its relation to hydrocarbon and mineral resources [Journal Article]. , *11*, 59-90.

Nakamura, K. (1977). Volcanoes as possible indicators of tectonic stress orientation?principle and proposal [Journal Article]. *Journal of Volcanology and Geothermal Research*, *2*(1), 1-16.

Nover, G. (2005). Electrical properties of crustal and mantle rocks - a review of laboratory measurements and their explanation [Journal Article]. *Surveys in Geophysics*, *26*(5), 593-651. Retrieved from <GotoISI>://WOS:000233262300004 doi: 10.1007/s10712-005-1759-6

Núñez, R. (2018). *Procesos de transporte de fluidos hidrotermales a lo largo de un sisterma de fallas: Geología estructural y modelamineto númerico con elementos de borde* (Thesis).

Pardo, M., Vera, E., Yáñez, G., & Monfret, T. (1967). Tomografía sísmica bajo los andes de chile central (33-34.5 s): Implicaciones sismotectónicas [Conference Proceedings]. In *Congreso geológico chileno* (p. S9-067).

Pavez, C., Tapia, F., Comte, D., Gutierrez, F., Lira, E., Charrier, R., & Benavente, O. (2016). Characterization of the hydrothermal system of the tinguiririca volcanic com-

plex, central chile, using structural geology and passive seismic tomography [Journal Article]. *Journal of Volcanology and Geothermal Research*, *310*, 107-117.

Pérez-Flores, P., Cembrano, J., Sánchez-Alfaro, P., Veloso, E., Arancibia, G., & Roquer, T. (2016). Tectonics, magmatism and paleo-fluid distribution in a strike-slip setting: Insights from the northern termination of the liquiñe?ofqui fault system, chile [Journal Article]. *Tectonophysics*, *680*, 192-210. Retrieved from `http://www.sciencedirect.com/science/article/pii/S0040195116301330` doi: https://doi.org/10.1016/j.tecto.2016.05.016

Pérez-Flores, P., Veloso, E., Cembrano, J., Sánchez-Alfaro, P., Lizama, M., & Arancibia, G. (2017). Fracture network, fluid pathways and paleostress at the tolhuaca geothermal field [Journal Article]. *Journal of Structural Geology*, *96*, 134-148.

Piquer, J., Berry, R. F., Scott, R. J., & Cooke, D. R. (2016). Arc-oblique fault systems: their role in the cenozoic structural evolution and metallogenesis of the andes of central chile [Journal Article]. *Journal of Structural Geology*, *89*, 101-117.

Piquer, J., Castelli, J. C., Charrier, R., & Yanez, G. (2010). The cenozoic of the upper teno river, cordillera principal, central chile: stratigraphy, plutonism and their relation with deep structures [Journal Article]. *Andean geology*, *37*(1), 32-53.

Piquer, J., Yáñez, G., Rivera, O., & Cooke, D. R. (2019). Long-lived crustal damage zones associated with fault intersections in the high andes of central chile [Journal Article]. *Andean Geology*, *46*(2), 223-239.

Pommier, A. (2014). Interpretation of magnetotelluric results using laboratory measurements [Journal Article]. *Surveys in Geophysics*, *35*(1), 41-84.

Pritchard, M. E., Jay, J. A., Aron, F., Henderson, S. T., & Lara, L. E. (2013). Subsidence at southern andes volcanoes induced by the 2010 maule, chile earthquake [Journal Article]. *Nature Geoscience*, *6*, 632. Retrieved from `https://doi.org/10.1038/ngeo1855` doi: 10.1038/ngeo1855https://www.nature.com/articles/ngeo1855#supplementary-information

Ramos, V. A. (2010). The tectonic regime along the andes: Present-day and mesozoic regimes [Journal Article]. *Geol. J*, *45*, 2-25.

Ramos, V. A., Litvak, V. D., Folguera, A., Spagnuolo, M., Ramos, V., Litvak, V., . . . Spagnuolo, M. (2014). An andean tectonic cycle: From crustal thickening to extension in a thin crust (34?37 sl) [Journal Article]. *Geoscience Frontiers*, *3*(5), 351-367.

Richards, J. P., Boyce, A. J., & Pringle, M. S. (2001). Geologic evolution of the escondida area, northern chile: A model for spatial and temporal localization of porphyry cu mineralization [Journal Article]. *Economic Geology*, *96*(2), 271-305. Retrieved from `https://dx.doi.org/10.2113/gsecongeo.96.2.271` doi: 10.2113/gsecongeo.96.2.271

Roquer, T., Arancibia, G., Rowland, J., Iturrieta, P., Morata, D., & Cembrano, J. (2017). Fault-controlled development of shallow hydrothermal systems: Structural and mineralogical insights from the southern andes [Journal Article]. *Geothermics*, *66*, 156-173. Retrieved from `http://www.sciencedirect.com/science/article/pii/S0375650516301948` doi: https://doi.org/10.1016/j.geothermics.2016.12.003

Rowland, J., & Sibson, R. (2004). Structural controls on hydrothermal flow in a segmented rift system, taupo volcanic zone, new zealand [Journal Article]. *Geofluids*, *4*(4), 259-283.

Rowland, J. V., & Simmons, S. F. (2012). Hydrologic, magmatic, and tectonic controls on hydrothermal flow, taupo volcanic zone, new zealand: Implications for the formation of epithermal vein deposits [Journal Article]. *Economic Geology*, *107*, 427-457.

Sánchez, P., Pérez-Flores, P., Arancibia, G., Cembrano, J., & Reich, M. (2013). Crustal deformation effects on the chemical evolution of geothermal systems: the intra-arc liquiñe-ofqui fault system, southern andes [Journal Article]. *International Geology Review*, *55*(11), 1384-1400.

Sanchez-Alfaro, P., Sielfeld, G., Van Campen, B., Dobson, P., Fuentes, V., Reed, A., . . . Morata, D. (2015). Geothermal barriers, policies and economics in chile- lessons for the andes [Journal Article]. *Renewable and Sustainable Energy Reviews*, *51*, 1390-1401.

Sernageomin. (2003). Servicio nacional de geologia y mineria [Journal Article].

Shaw, H. R. (1980). The fracture mechanisms of magma transport from the mantle to the surface [Journal Article]. *Physics of magmatic processes*, *64*, 201-264.

Sibson, R. H. (1967). Structural permeability of fluid-driven fault-fracture meshes [Journal Article]. *development*, *1967*.

Sibson, R. H. (1985). A note on fault reactivation [Journal Article]. *Journal of Structural Geology*, *7*(6), 751-754.

Sibson, R. H. (1996). Structural permeability of fluid-driven fault-fracture meshes [Journal Article]. *Journal of Structural Geology*, *18*(8), 1031-1042.

Sibson, R. H. (2004). Controls on maximum fluid overpressure defining conditions for mesozonal mineralisation [Journal Article]. *Journal of Structural Geology*, *26*, 1127-1136.

Sielfeld, G., Cembrano, J., & Lara, L. (2016). Transtension driving volcano-edifice anatomy: Insights from andean transverse-to-the-orogen tectonic domains [Journal Article]. *Quaternary International*.

Sielfeld, G., Lange, D., & Cembrano, J. (2019). Intra-arc crustal seismicity: Seismotectonic implications for the southern andes volcanic zone, chile [Journal Article]. *Tectonics*, *38*(2), 552-578.

Sillitoe, R. (1997). Characteristics and controls of the largest porphyry copper?gold and epithermal gold deposits in the circum?pacific region [Journal Article]. *Australian Journal of Earth Sciences*, *44*(3), 373-388.

Simpson, F., & Bahr, K. (2005). *Practical magnetotellurics* [Book]. Cambridge University Press.

Stanton-Yonge, A., Griffith, W., Cembrano, J., St Julien, R., & Iturrieta, P. (2016). Tectonic role of margin-parallel and margin?transverse faults during oblique subduction in the southern volcanic zone of the andes: Insights from boundary element modeling [Journal Article]. *Tectonics*, *35*(9), 1990-2013.

Stern, C., Moreno, H., López-Escobar, L., Clavero, J., Lara, L., Naranjo, J., . . . Skewes, M. (2007). Chilean volcanoes [Journal Article]. *The geology of Chile*, 149-180.

Suzuki, Y., Ioka, S., & Muraoka, H. (2014). Determining the maximum depth of hydrothermal circulation using geothermal mapping and seismicity to delineate the depth to brittle-plastic transition in northern honshu, japan [Journal Article]. *Energies*, *7*(5), 3503-3511.

Tardani, D., Reich, M., Roulleau, E., Takahata, N., Sano, Y., Pérez-Flores, P., . . . Arancibia, G. (2016). Exploring the structural controls on helium, nitrogen and carbon isotope signatures in hydrothermal fluids along an intra-arc fault system [Journal Article]. *Geochimica et Cosmochimica Acta*, *184*, 193-211.

Tassi, F., Aguilera, F., Benavente, O., Paonita, A., Chiodini, G., Caliro, S., . . . Vaselli, O. (2016). Geochemistry of fluid discharges from peteroa volcano (argentina-chile) in 2010?2015: Insights into compositional changes related to the fluid source region (s) [Journal Article]. *Chemical geology*, *432*, 41-53.

Teyssier, C., Tikoff, B., & Markley, M. (1995). Oblique plate motion and continental tectonics [Journal Article]. *Geology*, *23*(5), 447-450.

Tibaldi, A. (2005). Volcanism in compressional tectonic settings: Is it possible? [Journal Article]. *GEOPHYSICAL RESEARCH LETTERS*, *32*, L06309.

Tikoff, B., & Teyssier, C. (1994). Strain modeling of displacement-field partitioning in transpressional orogens [Journal Article]. *Journal of Structural Geology*, *16*(11), 1575-1588.

Turienzo, M., Dimieri, L., Frisicale, C., Araujo, V., & Sánchez, N. (2012). Cenozoic structural evolution of the argentinean andes at 3440?s: A close relationship between thick and thin-skinned deformation [Journal Article]. *Andean Geology*, *39*(2), 317-357.

Viramonte, J., Galliski, M., Araña Saavedra, V., Aparício, A., García Cucho, L., & Martín Escorza, C. (1984). El finivulcanismo básico de la depresión de arizaro, provincia de salta. 9 congreso geológico argentino, 5?9 november 1984, bariloche, argentina [Journal Article]. *Actas*, *3*, 234-251.

Wannamaker, P. E., Caldwell, T. G., Jiracek, G. R., Maris, V., Hill, G. J., Ogawa, Y., ... Heise, W. (2009). Fluid and deformation regime of an advancing subduction system at marlborough, new zealand [Journal Article]. *Nature*, *460*(7256), 733.

Wrage, J., Tardani, D., Reich, M., Daniele, L., Arancibia, G., Cembrano, J., ... Pérez-Moreno, R. (2017). Geochemistry of thermal waters in the southern volcanic zone, chile ? implications for structural controls on geothermal fluid composition [Journal Article]. *Chemical Geology*, *466*, 545-561. Retrieved from `http://www.sciencedirect.com/science/article/pii/S0009254117304023` doi: https://doi.org/10.1016/j.chemgeo.2017.07.004

Yáñez, G. A., Gana, P., & Fernández, R. (1998). Origen y significado geológico de la anomalía melipilla, chile central [Journal Article]. *Revista geológica de Chile*, *25*(2), 175-198.